Research Article

Journal of Environmental Nanotechnology

Synthesis of Biogenic Silver Nanoparticles from *Kalanchoe fedtschenkoi* Extract and Their Anticancer and Antibacterial Activities

Hrishikesh Khodade[1,4], Hiralal Sonawane[1], Deepak Shelke[2*], Mahadev Chambhare[2] and Kamlakar More[3]

[1]PG Research Centre in Botany, PDEA's Prof. Ramkrishna More ACS College (Affiliated to Savitribai Phule Pune University), Pune, MH, India
[2]Department of Botany, Amruteshwar Arts, Commerce and Science College, Pune, MH, India
[3]Department of Botany, Sant Gadge Baba Amravati University, Amravati, MH, India
[4]Department of Botany, S.M. Joshi College, Hadapsar, Pune, MH, India
Received: 25.06.2025 Accepted: 06.09.2025 Published: 30.09.2025
*dpk.shelke1@gmail.com

ABSTRACT

Green-synthesized nanoparticles are gaining widespread attention due to their eco-friendly production and broad biomedical potential. *Kalanchoe fedtschenkoi* Raym.-Hamet & H.Perrier, a widely cultivated medicinal plant, was explored in this study for its ability to mediate silver nanoparticle (AgNP) synthesis. Among leaf, root, stem, flower, and fruit, the leaf extract exhibited the most consistent and efficient synthesis, and was therefore selected for further analysis and biological evaluation. Silver nanoparticles synthesized using the leaf extract (Kf-L-AgNPs) were characterized by multiple analytical techniques. UV-Vis spectroscopy confirmed their formation with a characteristic SPR peak around 420 nm. The FESEM and TEM analyses revealed predominantly spherical nanoparticles with a size of around 25 nm. The HRTEM images showed clear lattice fringes, confirming their crystalline nature, while moderate agglomeration suggested interparticle interactions. Dynamic light scattering measurements indicated uniform size distribution, and Zeta Potential analysis revealed good colloidal stability with negative surface charges. X-ray diffraction studies confirmed the crystalline structure of pure metallic silver nanoparticles, and FTIR detected functional groups from the plant leaf extract involved in the reduction and capping processes. The EDS analysis confirmed silver as the dominant element along with bio-organic components from the extract. Biological evaluations demonstrated that Kf-L-AgNPs exhibit strong anticancer activity, with IC_{50} values of 34.81 µg/ml for MCF-7 (breast cancer) and 98.73 µg/ml for A549 (lung cancer) cell lines. Antibacterial assays revealed significant zones of inhibition against both *Escherichia coli* and *Staphylococcus aureus*, indicating broad-spectrum antimicrobial potential. Additionally, LC-MS-based metabolic profiling of the leaf extract identified key phytochemicals, *viz*., picein, lampranthin II, *p*-coumaroylputrescine, delavirdine, and (±)7-epi-jasmonic acid, which may have contributed to the synthesis and bioactivity of the nanoparticles. Kf-L-AgNPs synthesized *via* a green, plant-based approach show great promise as anticancer and antimicrobial agents, though further investigation is needed to explore their potential in pharmaceutical applications.

Keywords: Anticancer; Antimicrobial; Green synthesis; Phytochemical profiling; Silver nanoparticles.

1. INTRODUCTION

Nanoparticles have captured substantial interest due to their distinctive properties and broad spectrum of applications (Khan *et al.* 2019). These ultra-small particles, typically extending from 1 to 100 nanometers, exhibit extraordinary optical, electrical, and catalytic behaviors that differ significantly from their bulk material counterparts (Singh *et al.* 2022). This uniqueness renders them invaluable across various domains such as medicine, integrated circuit technology, catalytic reactions, and environmental restoration. Nanoparticles come in various forms, including nanoparticles made of metals like gold, silver, and platinum; metal oxides such as titanium dioxide and zinc oxide; and carbon-based nanoparticles, such as fullerenes, carbon nanotubes, graphene, and polymeric nanoparticles (Murthy *et al.* 2022). Each type has unique properties and applications, ranging from electronics and catalysis to drug delivery and environmental remediation (Sengul *et al.* 2020). Among these, silver nanoparticles (AgNPs) are the most widely researched due to their remarkable properties and wide range of applications (Mourdikoudis *et al.* 2018; Andrade *et al.* 2023; Shoaib *et al.* 2021). AgNPs exhibit remarkable antibacterial, anticancer, and antioxidant activities, making them highly valuable in medical and healthcare sectors (Sofi *et al*. 2022). AgNPs have become versatile nanomaterials with potential applications across multiple domains, such as medicine, electronics, catalysis, and environmental remediation. Their unique physicochemical properties, such as size-dependent optical and catalytic behavior, make them highly attractive for advanced technological applications (Khan, 2018; Yaraki *et al.* 2022).

Conventional methods of nanoparticle synthesis include chemical and physical techniques, which often include the utilization of hazardous chemicals and significant energy consumption, raising environmental and health concerns (Jamkhande *et al*. 2019). To address these issues, green synthesis methods, especially those utilizing plant extracts, have gained prominence as sustainable and eco-friendly alternatives (Gupta *et al.* 2023). These biological approaches harness the reducing and stabilizing power of plant phytochemicals, offering a cleaner and more efficient pathway to nanoparticle synthesis. This study focuses on exploiting the green synthesis route for creating AgNPs, highlighting its environmental benefits and potential for scalable production.

The medical applications of AgNPs have gained much attention because of their antibacterial, anticancer, and antioxidant properties (Netala *et al.* 2024). Their distinctive physicochemical characteristics, such as a small size and a large surface area, enable AgNPs to interact effectively with biological systems (Akter *et al.* 2018). Antibacterial activity against a wide range of pathogenic microorganisms makes AgNPs potential candidates for antimicrobial therapies (Patra *et al.* 2017). Additionally, their capability to selectively target cancer cells while sparing healthy tissues holds promise for anticancer treatments (Akhtar *et al.* 2015). Additionally, the antioxidant properties of AgNPs contribute to cellular protection and may have implications in combating oxidative stress-related diseases (Tee *et al.* 2016). Cancer continues to be one of the most daunting challenges in contemporary medicine, presenting a substantial threat to global health. Characterized by uncontrolled cell proliferation and the capacity to metastasize to distant organs, cancer can lead to severe health complications and death (Anand *et al.* 2023). Despite advances in treatment modalities such as surgery, chemotherapy, and radiation, the high mortality rate associated with various cancers underscores the urgent need for more effective and targeted therapies (Boshuizen *et al.* 2020). Breast cancer continues to be a primary contributor to mortality from cancer in women, necessitating effective treatments. The high mortality rate highlights the urgent need for advancements in targeted therapies. Moreover, the aggressive behavior and high metastatic potential of lung cancer make it one of the most challenging cancers to treat. Its prevalence and severity underline the importance of developing innovative and effective treatment strategies (Almeida *et al.* 2020; Song *et al*. 2020; Qu *et al.* 2021).

Bacterial infections pose a significant threat to human health, leading to severe illnesses and deaths worldwide (Janikddfghx *et al.* 2020). Antibacterial therapies work by targeting essential bacterial functions, thereby inhibiting their growth or killing them outright (Yin *et al.* 2015). However, the rise of antibiotic resistance has become a major concern, as many bacteria have evolved mechanisms to evade the effects of traditional antibiotics, rendering treatments less effective (Uddin *et al.* 2021). In this context, AgNPs have emerged as promising candidates due to their unique properties. AgNPs exhibit potent antibacterial properties, owing to their capability to break open the bacterial cell membranes, generate reactive oxygen species, and interfere with DNA duplication (Das *et al.* 2017). These multifaceted mechanisms of action make AgNPs less prone to resistance development, highlighting their potential as a powerful tool in combating antibiotic-resistant bacterial infections.

According to Coutinho *et al.* (2008) and Nascimento *et al*. (2023), the genus *Kalanchoe* is renowned for its diverse medicinal properties, with traditional uses encompassing treatments for skin conditions, inflammation, and respiratory ailments. The genus *Kalanchoe*, known for its rich bioactive compound content, has shown considerable potential in the green synthesis of nanoparticles (Aryan *et al.* 2021; Molina *et al.* 2019; Gul *et al.* 2023). These plants not only facilitate the eco-friendly synthesis of nanoparticles but also enhance their biomedical potential, leveraging their inherent medicinal properties to produce nanoparticles with multi-faceted health benefits. *Kalanchoe fedtschenkoi*, commonly known as lavender scallops or South American air plant, is a succulent plant species native to Madagascar and now widely distributed, including in parts of India such as Ranikhet (Uttarakhand) and Panchkula (Haryana) (Andrade *et al.* 2023). This perennial succulent, belonging to the family Crassulaceae, exhibits a mature size of 1-2 feet tall and wide, preferring full to partial sunlight and a well-drained soil mix (Smith *et al.* 2022).

Kalanchoe fedtschenkoi has a long history of medicinal use, further highlighting its relevance in both traditional and modern healthcare systems (Casanova *et al.* 2022). The rich variety of bioactive compounds in *Kalanchoe* plants, including *Kalanchoe fedtschenkoi*, has attracted significant interest in pharmacological research. These compounds, found in various plant parts such as leaves, stems, and roots, and useful for pharmaceutical and agricultural applications, contributing to the plant-based medical applications (Mejía *et al.* 2023). Beyond its medicinal significance, *Kalanchoe fedtschenkoi* plays a crucial ecological role as it is a xerophytic plant that shows Crassulacean Acid Metabolism, thriving in arid environments and contributing to soil conservation and ecosystem resilience (Shah *et al.* 2022). Its ability to attract pollinators and support biodiversity enhances the ecological balance in its habitats, highlighting its ecological importance (Smith, 2022).

The green synthesis of nanoparticles heavily relies on the phytochemical constituents of plants, which act as reducing and stabilizing mediators (Balčiūnaitienė *et al.* 2022). Liquid Chromatography-Mass Spectrometry

(LC-MS) is a valuable tool in this context, as it allows for the precise identification and quantification of these bioactive compounds (Alves *et al.* 2019). By providing detailed phytochemical profiles, LC-MS helps in the examination of the plant's chemical composition and its potential efficacy in nanoparticle synthesis.

In recent years, there has been a budding interest in environmentally friendly methods for nanoparticle synthesis and also their potential use in the biomedical fields. While the plant is traditionally known for its therapeutic applications, its role in the green synthesis of AgNPs remains largely unexplored. To assess its potential, we investigated the reductive capabilities of five different plant parts (leaf, root, stem, flower, and fruit) for nanoparticle synthesis. This comparative approach aimed to identify the particular part extract most effective in producing stable and functional nanoparticles. Therefore, the focus of this study is on LC-MS profiling of the plant and synthesis of silver nanoparticles using a green approach with *Kalanchoe fedtschenkoi* plant extract, and to assess their anticancer and antibacterial potential.

2. MATERIALS AND METHODS

2.1 Collection of Plant Material

The *Kalanchoe fedtschenkoi* plant material used in this study was initially collected from Loknete Ramdas Patil Dhumal Arts, Science & Commerce College, Rahuri, Maharashtra, India. The collected specimen (Authentication number- Bot/BGC-28/AUTH) was then cultivated in the botanical garden of S. M. Joshi College, Hadapsar, Pune, India. The plants were grown in well-drained soil with adequate sunlight exposure to ensure optimal growth and development. The mature leaves were harvested at peak vegetative growth for subsequent utilization in the synthesis of AgNPs.

2.2 Preparation of Plant Part Extracts

To prepare the plant part extracts separately, 5 grams of *Kalanchoe fedtschenkoi* plant parts (root, stem, flower, and fruit) were thoroughly washed with double-distilled water and cleaned to remove any surface impurities. The cleaned plant parts were then crushed separately using a mortar and pestle. The resultant plant material was mixed with double-distilled water and subjected to centrifugation at 5000 rpm for 15 minutes. The supernatant was carefully collected and further filtered through a 0.22-micron filter to remove any impurities and debris. The filtered (leaf, root, stem, fruit, and flower) extracts were then stored separately at 4 °C until further use in the synthesis of silver nanoparticles.

2.3 *K. fedtschenkoi*-mediated Silver Nanoparticle Synthesis (Kf-AgNPs)

The synthesis of AgNPs was carried out using a 1 mM aqueous solution of silver nitrate ($AgNO_3$) as the precursor. To assess the influence of different plant parts on nanoparticle formation, individual extracts of *Kalanchoe fedtschenkoi* roots, leaves, stems, flowers, and fruits were prepared and employed as a natural agent for reduction and stabilization. For a distinct synthesis reaction, each 10 mL of plant part extract was mixed with 25 mL of the 1 mM $AgNO_3$ solution separately. The reaction mixture was maintained at 70 °C and pH 7 for a duration of 3 hours (Ali *et al.* 2013). To ensure complete reduction of Ag^+ ions, the reaction was kept at constant stirring (Rónavári *et al.* 2021).

After 24 hours of incubation, the synthesized nanoparticles (Kf-AgNPs) were purified by centrifugation at 15,000 rpm for 15 minutes, followed by washing with distilled water and acetone. The resulting pellets were dried in a hot air oven at 80 °C and collected in sterile Eppendorf tubes for characterization and comparative evaluation (Raut *et al.* 2010). The synthesized AgNPs were assigned abbreviations based on the specific *Kalanchoe fedtschenkoi* plant parts used for their synthesis. Nanoparticles synthesized using the leaf extract were designated as Kf-L-AgNPs, while those derived from root, stem, flower, and fruit extracts were referred to as Kf-R-AgNPs, Kf-S-AgNPs, Kf-F-AgNPs, and Kf-T-AgNPs, respectively. This nomenclature was adopted to facilitate clear differentiation and comparative analysis among the samples.

2.4 Characterization of Kf-L-AgNPs

2.4.1 UV-Vis Spectroscopy

The optical properties of the nanoparticles were analyzed using UV-vis Spectroscopy. Nanoparticle suspensions in distilled water were prepared using different parts of the *Kalanchoe fedtschenkoi* plant, namely, root, leaf, stem, flower, and fruit extracts, and their absorbance spectra were recorded in the range 350 nm to 780 nm. In addition, the *Kalanchoe fedtschenkoi* plant leaf extracts prepared in distilled water were also analyzed independently over a wavelength range of 300 nm to 800 nm to observe the absorbance characteristics of the phytochemical constituents before nanoparticle synthesis.

2.4.2 Field Emission Scanning Electron Microscopy (FESEM)

The characterization was conducted for silver nanoparticles synthesized using five different plant part extracts of *Kalanchoe fedtschenkoi*: Kf-L-AgNPs (leaf), Kf-R-AgNPs (root), Kf-S-AgNPs (stem), Kf-F-AgNPs (flower), and Kf-T-AgNPs (fruit). The morphology and surface structure were examined using Field Emission Scanning Electron Microscopy (FESEM) at an accelerating voltage of 15 kV. Samples were prepared by drop-casting diluted nanoparticle suspensions onto a conductive substrate, followed by sputter-coating with

gold to enhance surface conductivity and imaging quality.

High-resolution images were captured to analyze the size, shape, surface texture, and distribution of the nanoparticles synthesized from each plant part extract. Imaging was performed using in-lens TLD, SE, and BSE detectors, achieving resolutions of 1.0 nm, 1.4 nm and 1.8 nm at 15 kV, 1 kV, and at 3 kV, respectively and 30 Pa. The FESEM system, operated using xT Microscope Control software, featured a Quick Loader load lock system for efficient and contamination-free sample handling.

2.4.3 Transmission Electron Microscopy (TEM)

Transmission Electron Microscopy (TEM) was employed to analyze the morphology, particle size, and crystalline nature of the silver nanoparticles synthesized using leaf extract (Kf-L-AgNPs). A small aliquot of the nanoparticle suspension was dispersed in ethanol and sonicated in an ultrasonic bath for 15 minutes to ensure uniform dispersion. At room temperature, a drop of this suspension was deposited onto a carbon-coated copper grid and allowed to air dry.

The samples were examined using a high-resolution TEM (HRTEM) instrument (make and model) operating at an accelerating voltage of 200 kV. HRTEM images were taken, and ImageJ software was used to analyze particle size and distribution.

2.4.4 Dynamic Light Scattering (DLS)

The particle size distribution and polydispersity index (PDI) of Kf-L-AgNPs were determined using Dynamic Light Scattering (DLS). The nanoparticles were redispersed in distilled water, and the suspensions were subjected to ultrasonication to ensure uniform dispersion and minimize agglomeration before analysis.

2.4.5 Zeta Potential Analysis (ZP)

The Zeta Potential (ZP) analysis of Kf-L-AgNPs was conducted using a Zetasizer Nano ZS instrument. The nanoparticle suspensions were prepared in distilled water, and ultrasonication was applied to achieve homogeneous dispersion before measurement. The analysis was performed to evaluate the electrophoretic mobility of the particles, from which Zeta Potential values were calculated. This examination gives valuable information about the surface charge and colloidal stability of the synthesized Kf-L-AgNPs, enhancing the understanding of their behavior in aqueous suspension systems.

2.4.6 X-ray Diffraction (XRD)

The crystalline structure of Kf-L-AgNPs was investigated using X-ray Diffraction (XRD) analysis. The measurements were performed on a Bruker D8 Advance diffractometer equipped with Cu Kα radiation (λ = 1.5406 Å), operating at an accelerating voltage of 40 kV and a current of 40 mA. Diffraction patterns were recorded over a 2θ range of 5° to 80° at a scanning speed of 2°/min, ensuring high-resolution detection of diffraction peaks. The dried Kf-L-AgNP powder was evenly spread onto a clean glass slide and scanned under the specified conditions. The resulting diffraction data were saved in .ras, .asc, and .xy formats using Bruker DIFFRAC.SUITE software. Phase identification was carried out by comparing the observed peak positions with standard reference patterns from the Joint Committee on Powder Diffraction Standards (JCPDS) database. The crystallite size of the nanoparticles was estimated using the Debye–Scherrer equation, based on the full width at half maximum (FWHM) of the most prominent peak, applying a shape factor (K) of 0.9.

2.4.7 Fourier-transform Infrared Spectroscopy (FTIR)

The surface chemistry and presence of functional groups associated with the biosynthesized silver nanoparticles (Kf-L-AgNPs) were examined using Fourier-Transform Infrared Spectroscopy (FTIR). The analysis was performed on a spectrometer equipped with an attenuated total reflectance (ATR) accessory, which minimized sample preparation requirements.

The dried nanoparticle powder was pressed into a thin film and directly applied to the ATR crystal. Spectra were recorded in the mid-infrared range of 4000–500 cm^{-1} to identify the functional groups responsible for the reduction of silver ions and the stabilization of the resulting nanoparticles. All measurements were taken at room temperature with a resolution of 4 cm^{-1}, and spectra were averaged over multiple scans to improve accuracy and reproducibility. This technique enabled the identification of bioactive compounds from the plant leaf extract, such as phenols, flavonoids, and proteins, which played a crucial role in nanoparticle synthesis.

2.4.8 Energy Dispersive Spectrometry (EDS)

The elemental composition and spatial distribution of the Kf-L-AgNPs were analyzed using Energy Dispersive Spectrometry (EDS) coupled with FESEM. The EDS system offered high-resolution elemental detection with an energy resolution of 123 eV at Mn Kα and 45 eV at C Kα.

This technique provided both qualitative and semi-quantitative analysis of the elemental constituents present in the synthesized nanoparticles. Data acquisition and processing were performed using Espirit 1.9 software, enabling accurate identification of elemental signals and generation of elemental mapping profiles. The EDS analysis confirmed the presence of elemental silver and other trace elements derived from plant

metabolites, supporting the successful biosynthesis and surface stabilization of Kf-L-AgNPs.

2.5 Cytotoxic Activity

The MTT assay was employed to evaluate the cytotoxic effects of Kf-L-AgNPs on two human cancer cell lines: MCF-7 (breast cancer) and A549 (lung cancer). The MCF-7 cell line, representing human breast adenocarcinoma (Catalog No. CKMTT328A), and the A549 cell line, representing human lung adenocarcinoma (Catalog No. CKMTT335), were acquired from the National Centre for Cell Science (NCCS), Pune, India. Both cell lines were cultured in Dulbecco's Modified Eagle Medium (DMEM) supplemented with 10% fetal bovine serum (FBS, MP Biomedicals, Germany) and antibiotics (penicillin–streptomycin). The cells were maintained at 37 ℃ in a humidified atmosphere containing 5% CO_2 and monitored to ensure exponential growth during experiments.

For cytotoxicity evaluation, Kf-L-AgNPs were tested at increasing concentrations ranging from 0.001 to 100 µg/mL against selected cell lines. Cells were cultured in T-25 flasks, trypsinized, and centrifuged at 300 × g to obtain a uniform cell pellet. The cell count was adjusted to approximately 10,000 cells per 200 µL using DMEM-high glucose (DMEM-HG) medium. Each 200 µL cell suspension was seeded into individual wells of a 96-well plate and incubated for 24 hours at 37 ℃ in a humidified atmosphere containing 5% CO_2. After the initial incubation, the culture medium was replaced with 200 µL of varying concentrations of Kf-L-AgNPs or the standard chemotherapeutic agent docetaxel (reference control). Following 24 hours of treatment exposure, cytotoxicity was assessed using the MTT assay. For this, the treatment medium was replaced with 200 µL of fresh medium containing 0.5 mg/mL MTT reagent, and the cells were incubated for 3 hours at 37 ℃. After incubation, the medium was aspirated, and 100 µL of DMSO was added to each well to dissolve the resulting formazan crystals.

The absorbance was measured at 570 nm (test wavelength) and 630 nm (reference wavelength) using a microplate reader (Model BK-EL10A, Biobase, China). The data were used to calculate percentage cell viability and growth inhibition, and IC_{50} values were determined from dose-response curves generated for both the nanoparticle treatment and the reference drug.

2.6 Antibacterial Activity

The antibacterial activity of Kf-L-AgNPs was assessed against both Gram-negative and Gram-positive strains, *Escherichia coli* and *Staphylococcus aureus*, respectively. The Mueller-Hinton Agar Medium was prepared from commercially available media (HiMedia Labs) and sterilized through autoclaving. After cooling to a temperature range of 40-50 ℃, the medium was poured aseptically into sterile Petri plates to a uniform depth of 4 mm. For the inoculation process, single colonies from pure cultures of *E. coli* and *S. aureus* were picked and suspended in 5 mL of nutrient broth. These broths were incubated at 37 ℃ until obtaining an absorbance of 1.0 at 600 nm, serving as standardized inocula. Sterile cotton swabs were then dipped into the standardized inoculums, and excess inoculum was removed by lightly pressing the swab against the tube wall. The Mueller-Hinton Agar plates were inoculated by streaking with the swabs containing the inoculum to ensure even distribution. Test samples, including high concentration (1 mg/mL) and low concentration (0.1 mg/mL) of Kf-L-AgNPs, along with the plant leaf extract, were prepared. Standard antibiotics, tetracycline and kanamycin, were used as controls for comparison. Using sterile forceps, the test samples and the antibiotic discs were placed on the surface of the inoculated plates, ensuring complete contact with the agar surface. The plates were then incubated at 37 ℃ for 18 hours.

2.7 LCMS Analysis

The fresh plant leaves (10 g) were crushed in liquid nitrogen by mortar and pestle. The resultant powder was dissolved in 30 mL of methanol. This mixture was kept overnight on a shaker (Gegengeimer, 1990). Then, it was filtered using a 0.22-µm syringe filter to eliminate the particulate matter. For the LC-MS analysis, the concentrated methanolic extracts were re-dissolved in HPLC-grade methanol to a final concentration of 1 mg/mL. The analysis was performed using an Agilent 6200 series TOF/6500 series Q-TOF B.09.00 system equipped with a ZORBAX Eclipse Plus C18 column (4.6 x 150 mm, 3.5 µm). The mobile phase consisted of a mixture of water with 0.1% formic acid (A) and acetonitrile with 0.1% formic acid (B). The gradient program started with 5% B, increasing to 95% B over 30 minutes. The flow rate was set to 0.3 mL/min, with an injection volume of 10 µL. The ionization was carried out using Electrospray Ionization (ESI) in positive mode, covering a mass range of m/z 100-1500. The source parameters included a capillary voltage of 3500 V, a drying gas flow of 10 L/min, a gas temperature of 300°C, and a nebulizer pressure of 35 psi. The spectra were compared with the library for compound identification.

2.8 Statistical Analysis

Antibacterial and cytotoxicity activities were accomplished with three replicates. The data underwent one-way analysis of variance (ANOVA) using SPSS 16.0 software, followed by Duncan's multiple range test (DMRT) to identify significant differences at a confidence level of $p < 0.05$. The variability in data observations was presented as mean ± standard error (SE). The significant differences in cytotoxicity activities between the two drugs were analyzed using a Student's t-test at a significance level of $p \leq 0.05$.

3. RESULTS

3.1 Characterization of Kf-AgNPs

3.1.1 Surface Plasmon Resonance (SPR)

The biosynthesis of silver nanoparticles using *Kalanchoe fedtschenkoi* plant part extracts was visually confirmed by a distinct color change in the reaction mixture (Fig. 1). The change in color from colorless to pale yellow, and finally to various shades of brown was observed, depending on the plant part used. This visible color change occurred progressively over the 3-hour reaction period and is attributed to the excitation of Surface Plasmon Resonance (SPR) in the synthesized nanoparticles. The brown coloration, a characteristic of AgNP formation, indicates the successful reduction of Ag^+ ions and formation of colloidally stable silver nanoparticles.



Fig. 1: Visible color change in silver nitrate solutions after treatment with *Kalanchoe fedtschenkoi* plant part extracts, indicating AgNP formation through SPR. Samples include: (a) Kf-L-AgNPs (leaf), (b) Kf-F-AgNPs (flower), (c) Kf-S-AgNPs (stem), (d) Kf-T-AgNPs (fruit), and (e) Kf-R-AgNPs (root)

3.1.2 UV-Vis Spectroscopy

To validate the synthesis of silver nanoparticles and assess the optical characteristics of different plant part extracts, UV-Vis spectroscopy was performed on nanoparticles synthesized using extracts of *Kalanchoe fedtschenkoi*. The AgNP solutions demonstrated a sharp and well-defined absorbance peak at 420 nm (Fig. 2a), which is characteristic of the SPR of AgNPs. The SPR peaks for all five extracts occurred at nearly the same wavelength and showed comparable spectral intensity. The consistency in SPR peak position suggests that all plant part extracts were effective in reducing Ag^+ ions and stabilizing the resulting nanoparticles. Among these, no significant spectral shift was observed, indicating similarity in nanoparticle formation irrespective of the plant part used.

For comparison, the UV-Vis spectra of silver nitrate solution, distilled water, and *K. fedtschenkoi* leaf extract were also recorded (Fig. 2b). The leaf extract exhibited a broad absorbance across the visible spectrum, likely due to the presence of phytochemicals such as flavonoids, terpenoids, and phenolic compounds. In contrast, silver nitrate solution and distilled water showed negligible absorbance, confirming that the SPR peak observed near 420 nm was specific to the formation of silver nanoparticles (Fig. 2c and d). These results confirm the successful green synthesis of AgNPs and emphasize the reduction and stabilizing role of phytoconstituents present in various parts of *Kalanchoe fedtschenkoi*.

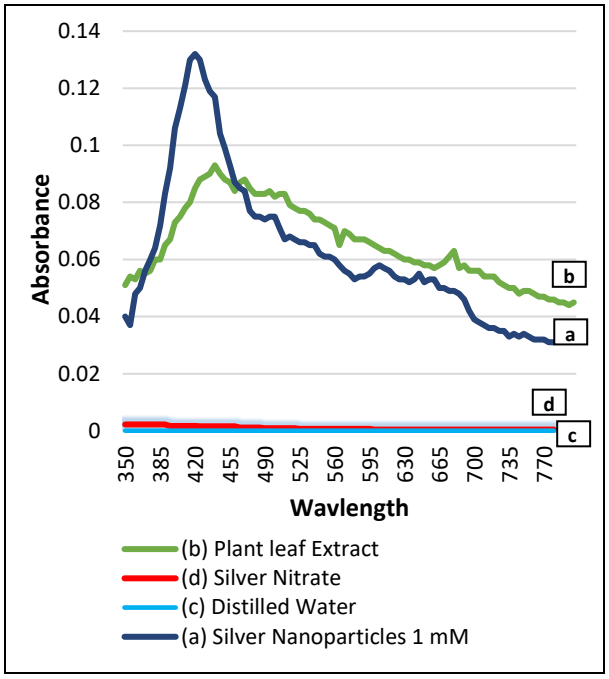


Fig. 2(a): UV-Vis spectrum of Kf-L-AgNPs synthesized using 1.0 mM silver nitrate (characteristic SPR peaks around 420 nm), (b) *Kalanchoe fedtschenkoi* plant leaf extracts absorption pattern, (c) Absorption spectrum of distilled water, and (d) Absorbance spectrum of silver nitrate

3.1.3 Field Emission Scanning Electron Microscopy (FESEM)

The characterization of Kf-AgNPs using FESEM revealed distinct morphologies and particle sizes depending on the *K. fedtschenkoi* plant part extract used in the synthesis (Fig. 3). Kf-L-AgNPs displayed spherical shapes with average sizes 16.78 nm (Fig. 3a). Kf-F-AgNPs had a size around 32 nm (Fig. 3b), while KF-S-AgNPs showed an average size of 20 nm in (Fig. 3c). Similarly, Kf-T-AgNPs produced using fruit extract showed an average size of 19 nm (Fig. 3d), and root extract based Kf-R-AgNPs exhibited a broader size of 34 nm (Fig. 3e), although all samples showed predominantly spherical shapes with an overall average size of approximately 25 nm.

3.1.4 Transmission Electron Microscopy (TEM)

The TEM analysis of the Kf-L-AgNPs revealed a predominantly spherical to quasi-spherical morphology with a narrow size distribution (Fig. 4). The particle sizes ranged from 5 nm to 50 nm, with an average size of approximately 25 nm. HRTEM images showed well-

defined lattice fringes, confirming the crystalline nature of the nanoparticles. The measured interplanar spacing (d-spacing) was consistent with reported values for metallic silver (Ag^0), indicating good phase purity and structural order. Some moderate agglomeration was observed, likely resulting from interparticle interactions during the drying process. Although Selected Area Electron Diffraction (SAED) data are not shown here, the visible lattice fringes and particle arrangement support the polycrystalline nature of the synthesized nanoparticles. These observations confirm the successful biosynthesis of well-crystallized Kf-L-AgNPs with controlled size and morphology using *Kalanchoe fedtschenkoi* leaf extract.

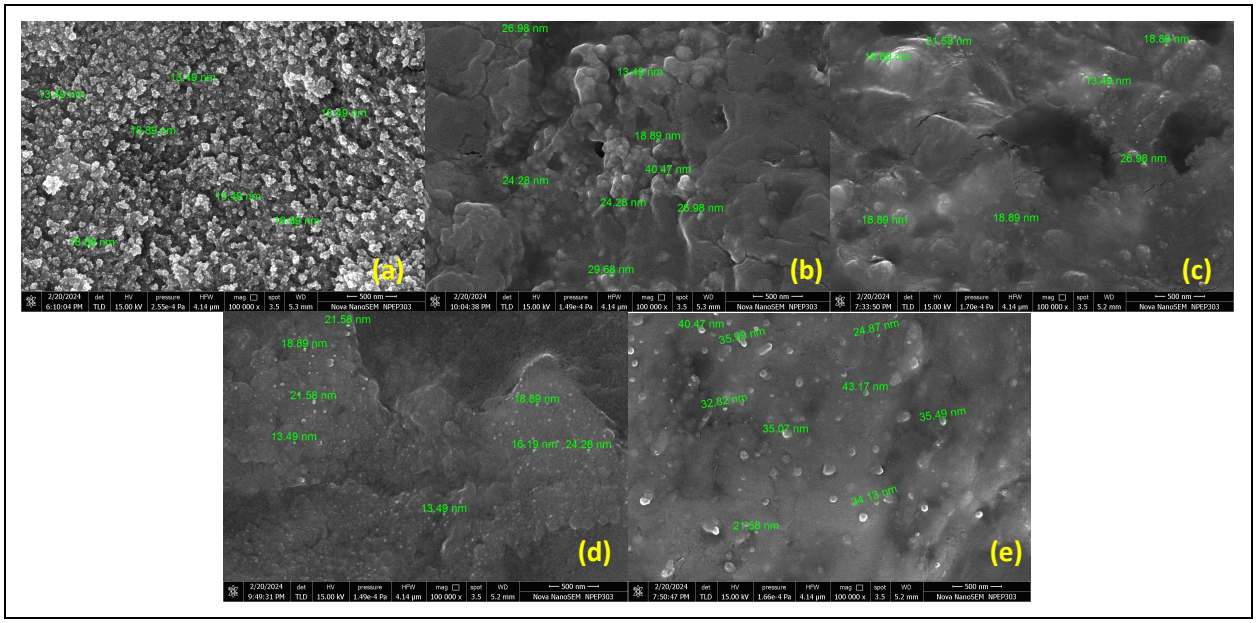


Fig. 3: FESEM images of Kf-AgNPs synthesized using different *K. fedtschenkoi* plant part extracts: (a) Kf-L-AgNPs (leaf), (b) Kf-F-AgNPs (flower), (c) Kf-S-AgNPs (stem), (d) Kf-T-AgNPs (fruit), and (e) Kf-R-AgNPs (root)

Table 1. Dynamic Light Scattering (DLS) analysis of Kf-L-AgNPs

Sample ID	Eff. Diam. (nm)[a]	PDI[b]
Kf-L-AgNPs sample-1	77.86	0.0482
Kf-L-AgNPs sample-2	71.83	0.0445
Kf-L-AgNPs sample-3	49.01	0.0303
Mean	66.23	0.0410
Std. Error	12.42	0.0078
Std. Deviation	7.17	0.0045

[a]Effective diameter refers to the average hydrodynamic size of nanoparticles measured in solution.
[b]PDI reflects the uniformity of particle size distribution; values < 0.1 suggest monodispersity.

3.1.5 Dynamic Light Scattering (DLS) Analysis

The DLS analysis of the Kf-AgNPs exhibited varying effective diameters across different samples (Fig. 5). Sample 1 showed an effective diameter of 77.86 nm; samples 2 and 3 registered 71.83 nm and 49.01 nm, respectively (Table 1). These measurements indicate a range of nanoparticle sizes with sample-specific variations. The PDI values were 0.482, 0.445, and 0.303 for samples 1, 2, and 3, respectively, suggesting relatively uniform size distributions within each sample. The baseline index was consistently recorded as 0.0 for all samples, indicating stable and monodisperse nanoparticle suspensions.

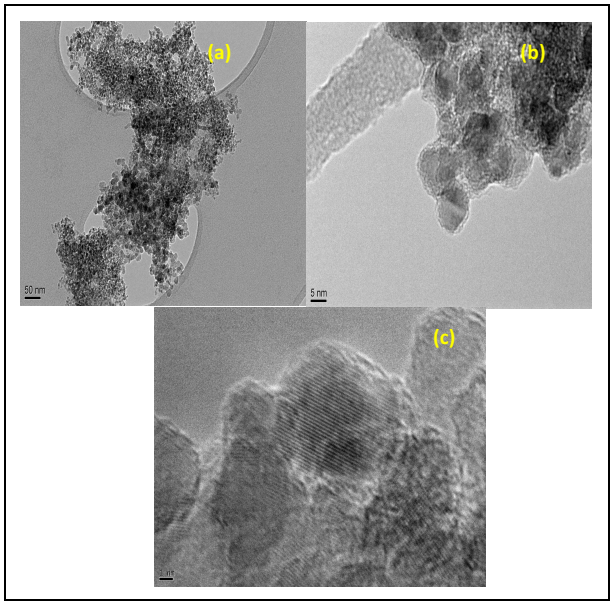


Fig. 4: TEM analysis of Kf-L-AgNPs: (a) low magnification (scale bar = 50 nm), (b) high magnification (scale bar = 5 nm), and (c) HRTEM image (scale bar = 1 nm)

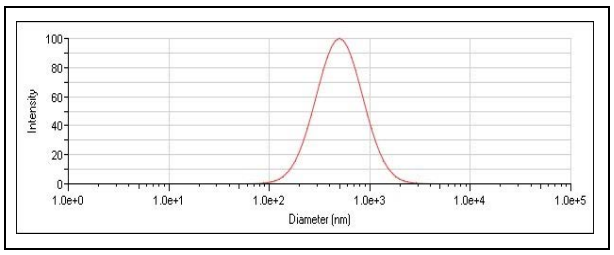


Fig. 5: Dynamic Light Scattering (DLS) size distribution graph of Kf-L-AgNPs

3.1.6 Zeta Potential (ZP) Analysis

The Zeta Potential (ZP) analysis of the synthesized Kf-L-AgNPs revealed negatively charged nanoparticles, indicating moderate colloidal stability in aqueous suspension. As shown in Fig. 6, the phase vs. time graph reflects consistent electrophoretic behavior, while the phase distribution with multiple data points indicates slight variability across measurements. Quantitative ZP values for three independently prepared samples ranged from –4.69 mV to –18.62 mV (Table 2), with a mean ZP of –11.34 mV ± 4.03. The corresponding electrophoretic mobility ranged from –0.37 to –1.46 (µm/s)/(V/cm), with a mean value of –0.89 ± 0.32. The Root Mean Square (RMS) residuals of the measurements remained low (mean = 0.0467), confirming the reliability and goodness of curve fitting in the data analysis. Although the average ZP value did not exceed ±30 mV, which is typically considered the threshold for high colloidal stability, it still indicates a moderate electrostatic repulsion among particles that may contribute to temporary stability in suspension. These values suggest that the Kf-L-AgNPs maintain sufficient dispersion under aqueous conditions, suitable for further biomedical and catalytic applications.

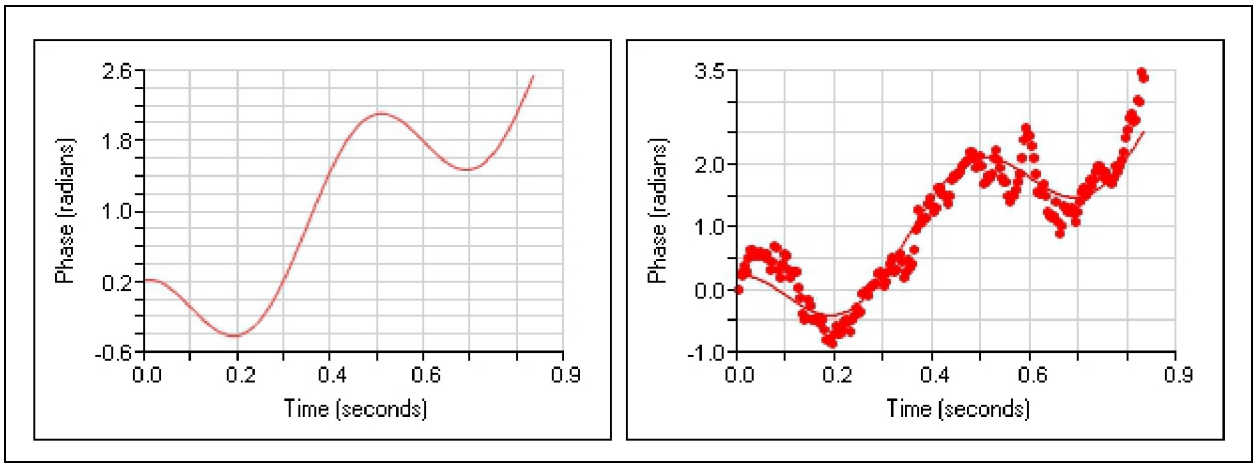


Fig. 6: Zeta potential distribution of Kf-L-AgNPs

Table 2. Zeta Potential (ZP) measurements of Kf-L-AgNPs

Sample ID	ZP (mV)[a]	Mobility (µ/s)/(V/cm)[b]	RMS Residual [c]
Kf-L-AgNPs sample-1	–4.69	–0.37	0.021875
Kf-L-AgNPs sample-2	–18.62	–1.46	0.055160
Kf-L-AgNPs sample-3	–10.72	–0.84	0.063008
Mean	–11.34	–0.89	0.046681
Std. Error	4.03	0.32	0.012608
Std. Deviation	6.99	0.55	0.021838

[a]Zeta potential indicates the surface charge of nanoparticles, where values > ±30 mV suggest good colloidal stability.
[b]Mobility refers to electrophoretic movement under applied voltage.
[c]RMS residual represents curve fitting error during zeta analysis.

3.1.7 XRD

The XRD pattern of the synthesized Kf-L-AgNPs is shown in Fig. 7. The analysis was performed using Cu Kα radiation (λ = 1.5406 Å) over a 2θ range of 5°–80°. Distinct diffraction peaks were observed at 2θ ≈ 38.1°, 44.3°, 64.4°, and 77.3°, corresponding to the (111), (200), (220), and (311) planes of face-centered cubic (fcc) metallic silver (Ag+), in accordance with JCPDS Card No. 04-0783. These peaks confirm the crystalline nature of the synthesized nanoparticles and validate the successful formation of pure metallic silver rather than silver oxide. The sharpness and high intensity of the peaks indicate high crystallinity and phase purity. Using the Debye–Scherrer equation applied to the (111) peak at 38.1°, the average crystallite size was calculated to be approximately 28.02 nm, suggesting the nanoparticles are in the nanocrystalline range. Based on the dominance of the (111) reflection, the particles likely exhibit spherical or quasi-spherical morphology, which is commonly observed in biosynthesized silver nanoparticles. These results confirm that the green

synthesis using *K. fedtschenkoi* leaf extract effectively produces well-crystallized, spherical silver nanoparticles suitable for further functional studies.

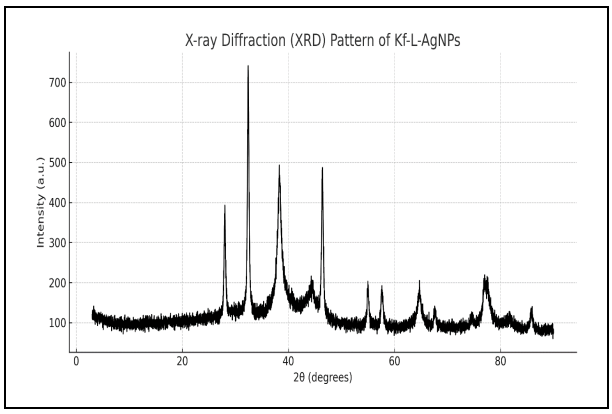


Fig. 7: X-ray diffraction (XRD) pattern of Kf-L-AgNPs

3.1.8 FTIR

The FTIR analysis of synthesized silver nanoparticles using *K. fedtschenkoi* leaf extract confirms the active involvement of various phytochemicals in the process of bioreduction and stabilization process (Fig. 8). A broad peak observed at 3429.20 cm^{-1} corresponds to O–H stretching vibrations, indicating the presence of hydroxyl groups from phenolic and alcoholic compounds in the leaf extract of *K. fedtschenkoi*, which likely acted as effective reducing agents during nanoparticle synthesis. The peaks at 2920.75 cm^{-1} and 2853.31 cm^{-1} are attributed to aliphatic C–H stretching, suggesting the presence of organic molecules that may function as surface modifiers or structural components in Kf-L-AgNPs. A strong absorption at 1700.81 cm^{-1} is assigned to carbonyl (C=O) stretching vibrations, typically found in carboxylic acids and aldehydes, and is considered responsible for reducing silver ions (Ag^{+}) to metallic silver (Ag^{0}). The band at 1582.19 cm^{-1}, related to N–H bending or aromatic C=C stretching, implies the presence of flavonoids or amino groups, which are known for their role in nanoparticle capping. Peaks at 1489.31 cm^{-1} and 1412.30 cm^{-1} correspond to aromatic ring and COO^{-} symmetric stretching, respectively, highlighting the contribution of tannins, flavonoids, and carboxylate compounds from *K. fedtschenkoi* in stabilizing the nanoparticle surface. Additional bands at 1241.20 cm^{-1} and 1129.86 cm^{-1} reflect C–O and C–N stretching vibrations, suggesting the involvement of esters, proteins, or amines as potential capping agents in Kf-L-AgNPs. Peaks at 1018.54 cm^{-1} and 888.68 cm^{-1}, associated with C–O–C linkages and aromatic C–H bending, point to the presence of polysaccharides and other plant-based aromatic compounds in the synthesis matrix. Most importantly, the distinct peak at 661.53 cm^{-1}, corresponding to metal–oxygen (Ag–O) stretching, provides conclusive evidence for the formation of AgNPs. These findings clearly indicate that the bioactive molecules in leaf extract promote stable Kf-L-AgNP formation.

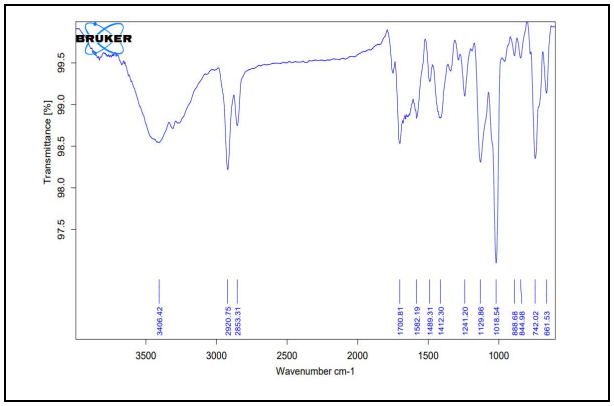


Fig. 8: FTIR spectrum of Kf-L-AgNPs revealing functional groups involved in the green synthesis and stabilization of AgNPs

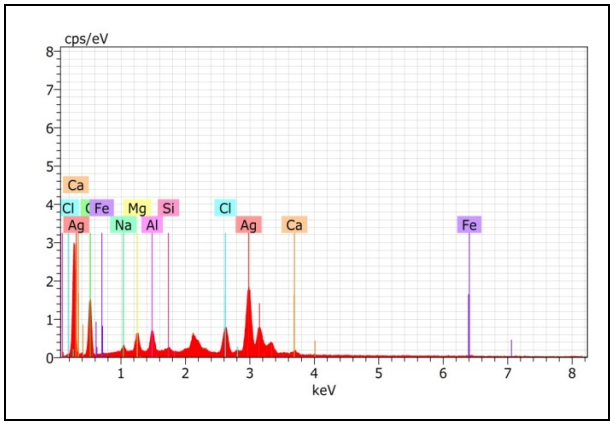


Fig. 9: EDS spectrum of Kf-L-AgNPs

3.1.9 Energy Dispersive Spectroscopy (EDS)

The EDS analysis of the synthesized Kf-L-AgNPs confirmed a substantial silver (Ag) content of 61.10%, with a prominent characteristic absorption peak at 3 keV, validating the presence of elemental silver in the sample (Fig. 9). This high silver concentration indicates the efficient bioreduction of Ag^{+} ions by phytochemicals present in the *K. fedtschenkoi* leaf extract, supporting the successful formation of silver nanoparticles. In addition to silver, the EDS spectra revealed the presence of oxygen (O) in the range 23–25%, and carbon (C) ranging from 14–16%. The oxygen content may originate from oxidized silver species (Ag_2O) or oxygen-containing functional groups from the plant leaf extract, while carbon likely reflects the organic matrix and capping agents derived from secondary metabolites such as flavonoids, phenols, and sugars.

Minor signals of other elements, including aluminum (Al), nitrogen (N), iron (Fe), sodium (Na), and magnesium (Mg), were also detected in trace amounts.

These may arise from residual components of the plant leaf extract or trace impurities. The elemental composition confirms the complex surface chemistry of the biosynthesized nanoparticles and reflects the multi-component nature of the *K. fedtschenkoi*-mediated reduction process.

3.2 Cytotoxic Activity

The absorbance of purple formazan measured spectrophotometrically revealed the extent of Kf-L-AgNPs-induced cytotoxicity. The synthesized Kf-L-AgNPs displayed remarkable cytotoxicity against MCF-7 breast cancer cells, indicating potent anticancer properties (Fig. 10 and Fig. 11). The IC_{50} values for the treatments were determined as follows: docetaxel, IC_{50} = 13.73 µg/mL; Kf-L-AgNPs, IC_{50} = 34.81 µg/mL. This comparison highlights the substantial anticancer efficacy of both standard (docetaxel) and Kf-L-AgNPs, with Kf-L-AgNPs showing notable effectiveness in reducing cell viability in a dose-dependent manner (Fig. 11). In the case of A549 lung cancer cells, the Kf-L-AgNPs also exhibited robust cytotoxic effects (Fig. 12). The IC_{50} values for A549 cells were found to be 33.09 µg/mL (for docetaxel) and Kf-L-AgNPs = 98.73 µg/mL. The dose-response curves for both treatments further confirmed the significant inhibition of cell growth by Kf-L-AgNPs (Fig. 13). Preliminary results suggest that Kf-L-AgNPs exhibit dose-dependent cytotoxicity against both MCF-7 and A549 cell lines, with higher concentrations resulting in significant reductions in cell viability.

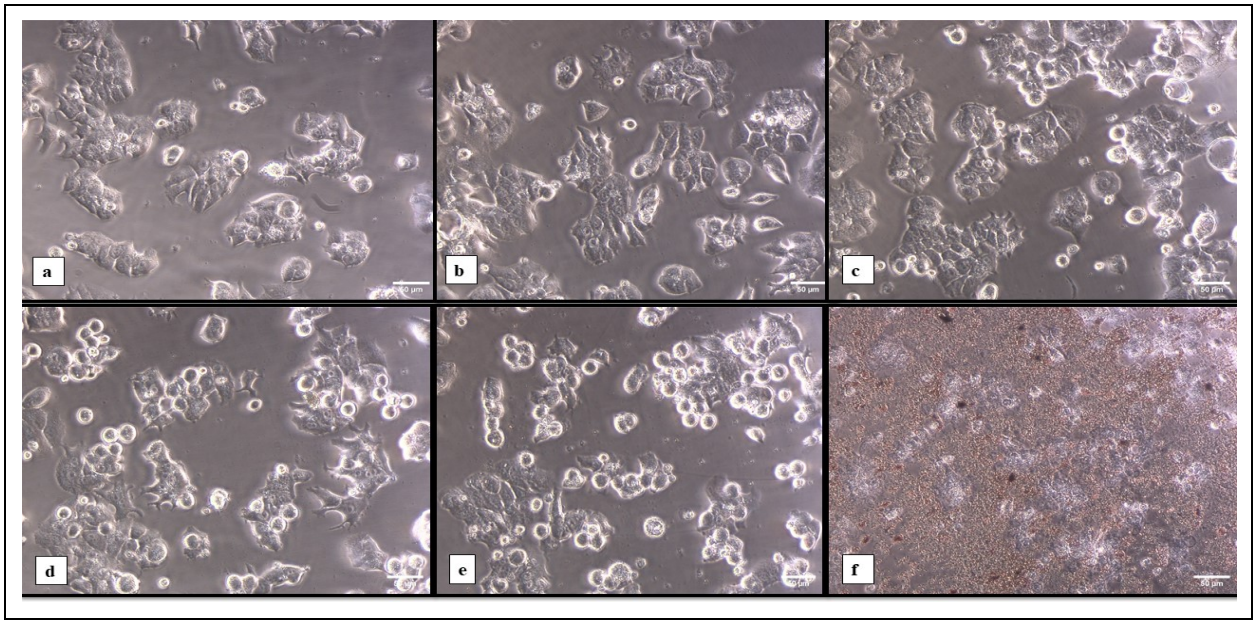


Fig. 10: Effect of increasing concentrations of Kf-L-AgNPs on MCF-7 breast cancer cells: (a) 0.001 µg/mL, (b) 0.01 µg/mL, (c) 0.1 µg/mL, (d) 1 µg/mL, (e) 10 µg/mL, and (f) 100 µg/m

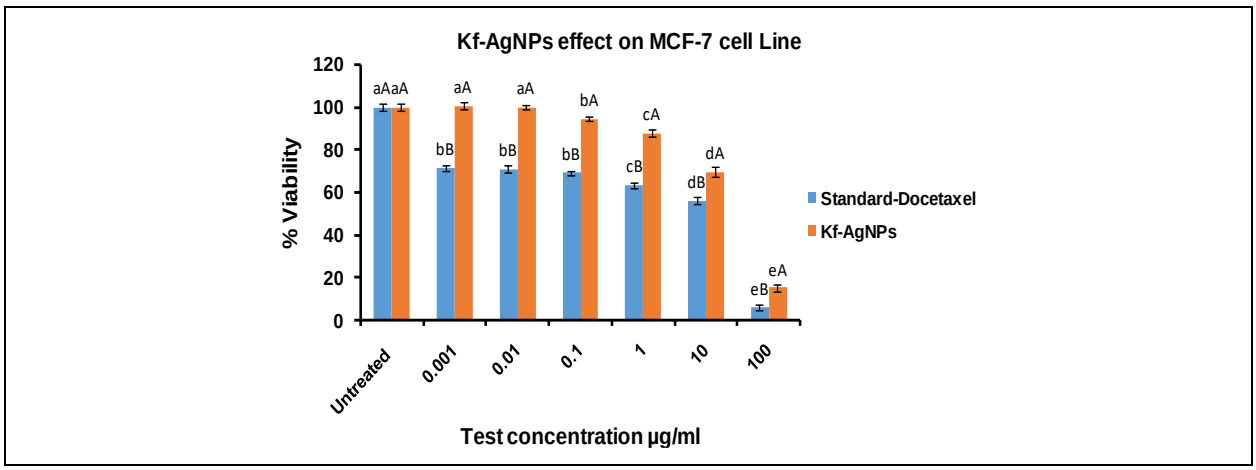


Fig. 11: Percent cell viability of MCF-7 cells after treatment with various concentrations of Kf-L-AgNPs; lowercase letters indicate significant differences between concentrations and uppercase letters show differences between test drugs ($p \leq 0.05$)

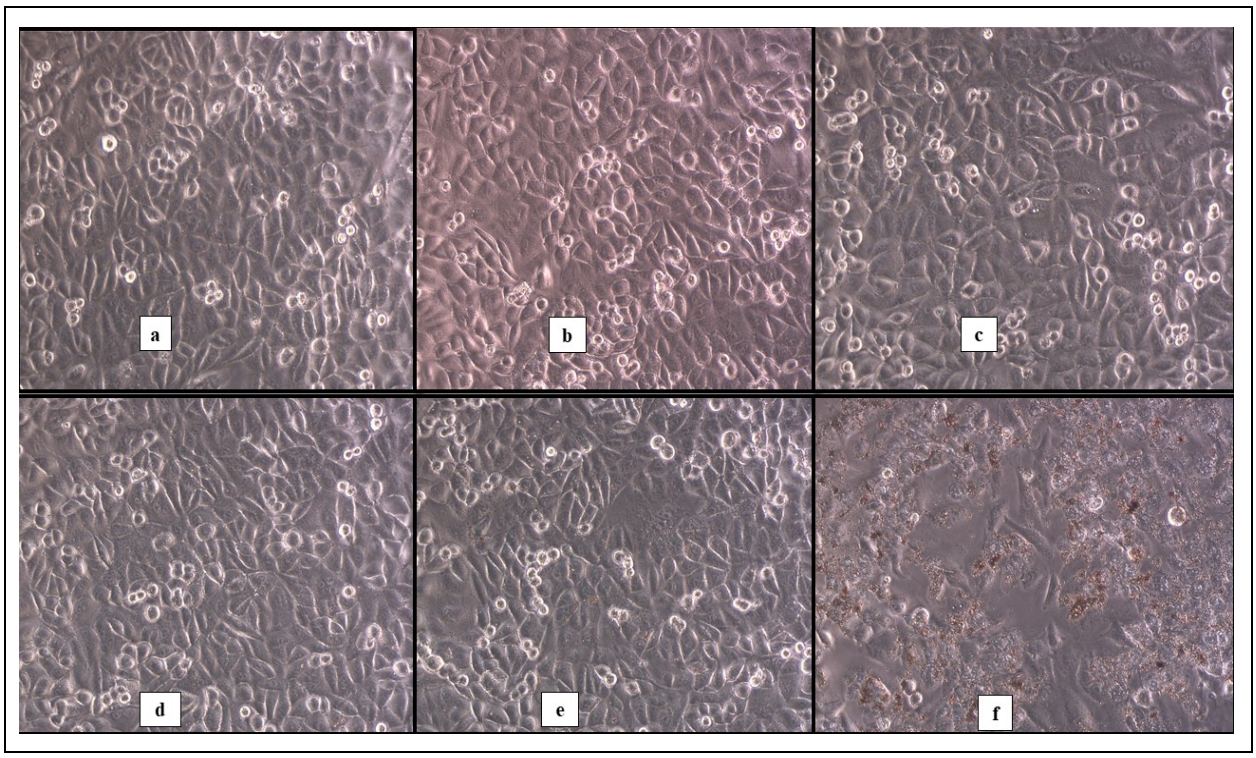


Fig. 12: Effect of increasing concentrations of Kf-L-AgNPs on A549 lung cancer cells: (a) 0.001 µg/mL, (b) 0.01 µg/mL, (c) 0.1 µg/mL, (d) 1 µg/mL, (e) 10 µg/mL, and (f) 100 µg/m

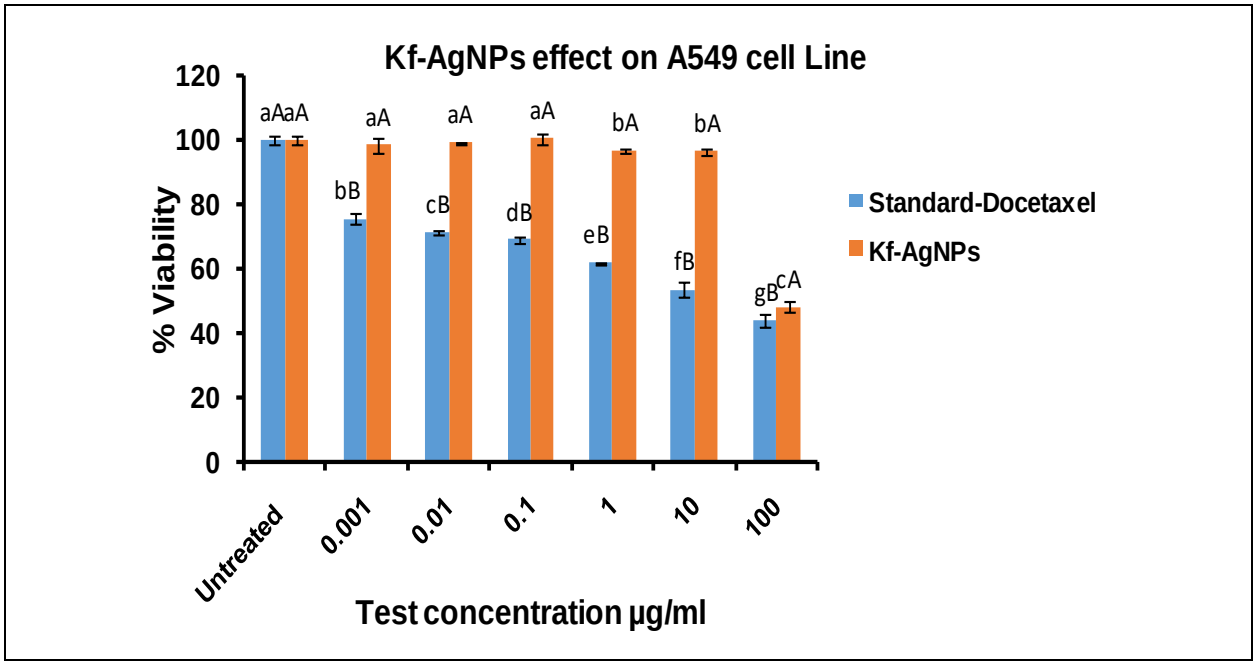


Fig. 13: Percent cell viability of A549 cells after treatment with various concentrations of Kf-L-AgNPs; lowercase letters indicate significant differences between concentrations and uppercase letters show differences between test drugs ($p \leq 0.05$)

3.3 Antimicrobial Activity

The antimicrobial efficacy of the Kf-L-AgNPs was determined by observing the zone of inhibition around the test organism after 18 hours of incubation. The results demonstrated significant antimicrobial activity of the Kf-L-AgNPs against both *S. aureus and E. coli* (Table 3). For *Staphylococcus aureus*, the high concentration of Kf-L-AgNPs (1 mg/mL) resulted in an inhibition zone of 22±0.735 mm, and the low

concentration (0.1 mg/mL) produced a zone of 21±0.694 mm. The plant leaf extract showed a modest inhibition zone of 19±0.854 mm. The control antibiotics, tetracycline and kanamycin, demonstrated inhibition zones of 28±0.845 mm and 18±0.521 mm, respectively (Fig. 14). For *Escherichia coli*, the high concentration of Kf-L-AgNPs (1 mg/mL) exhibited a substantial zone of inhibition measuring 25±0.582 mm, while the low concentration of Kf-L-AgNPs (0.1 mg/mL) displayed a zone of inhibition of 21±0.771 mm. The plant leaf extract showed a comparatively smaller zone of inhibition of 10±0.534 mm. In comparison, the control antibiotics, tetracycline and kanamycin, showed inhibition zones of 30±0.641 mm and 25±0.423 mm, respectively (Fig. 15). These results highlight the remarkable antibacterial potential of Kf-L-AgNPs, particularly at higher concentrations, demonstrating their effectiveness.

Table 3. Antibacterial activity of Kf-L-AgNPs, plant leaf extract, and standard antibiotics (values are expressed as mean ± SE; different superscript letters in the same column (a-d) indicate statistically significant ($p < 0.05$) differences)

Test Material	*E. coli*	*S. aureus*
	Zone diameter (mm)[a]	Zone diameter (mm)[a]
Tetracycline	30±0.641a	28±0.845a
Kanamycin	25±0.423b	18 ±0.521c
Plant Leaf Extract	10±0.534d	19±0.854c
Kf-L-AgNPs - Low Conc. (0.1 mg/ml)	21±0.771c	21±0.694b
Kf-L-AgNPs - High Conc. (1 mg/ml)	25±0.582b	22±0.735b

3.4 LC-MS Analysis of *Kalanchoe fedtschenkoi* Leaf Extract

The LC-MS analysis (Fig. 16) of *K. fedtschenkoi* leaves revealed a diverse array of secondary metabolites, as summarized in Table 4. Phenolic compounds identified included picein (Mass: 298.1040) and *p*-coumaroylputrescine (Mass: 234.1367), known for their antioxidant properties. Flavonoids such as lampranthin II (Mass: 727.1986) were also detected, contributing to the plant's potential therapeutic effects. Terpenes identified included (±)7-epi jasmonic acid (Mass: 210.1259), highlighting the plant's anti-inflammatory potential. Additionally, nitrogen-containing compounds like 1,3,7-trimethyluric acid (Mass: 210.0747) and delavirdine (Mass: 456.1941) are notable for their bioactivity. The presence of complex molecules such as dihydrozeatin riboside (Mass: 353.1688) and aculeacin A (Mass: 1078.5803) has also been reported.

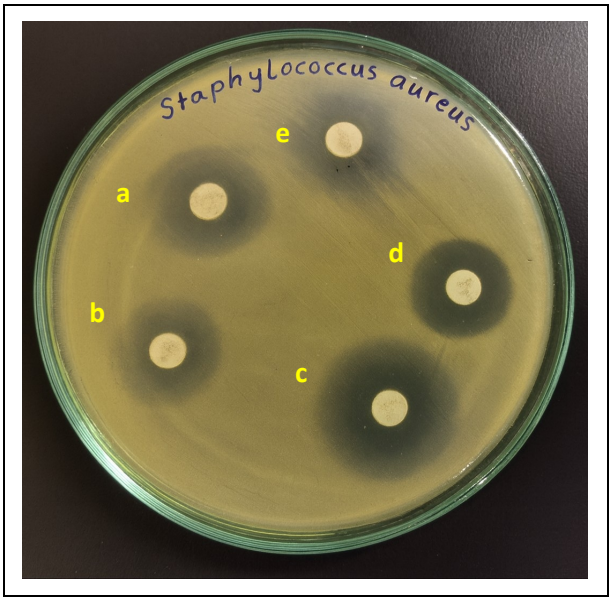


Fig. 14: Zone of inhibition against *S. aureus*: (a) Kf-L-AgNPs high (1 mg/mL), (b) Kf-L-AgNPs low (0.1 mg/mL), (c) tetracycline, (d) kanamycin, and (e) plant leaf extract

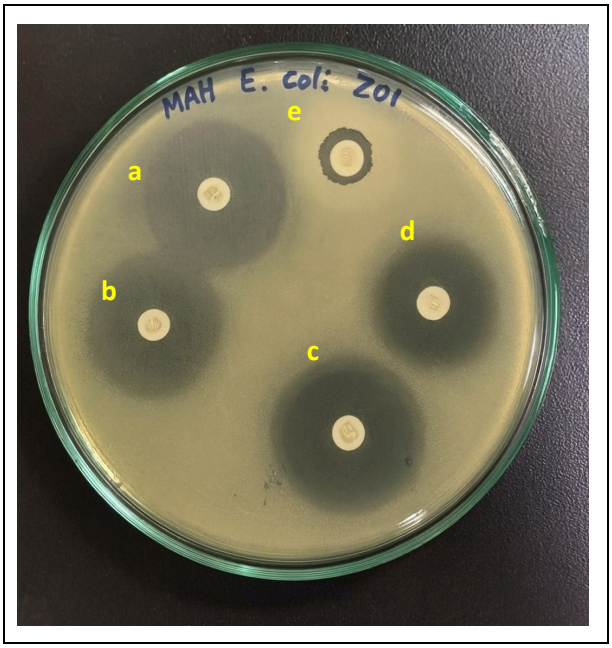


Fig. 15: Zone of inhibition against *Escherichia coli*: (a) tetracycline, (b) kanamycin, (c) Kf-L-AgNPs high (1 mg/mL), (d) Kf-L-AgNPs low (0.1 mg/mL), and (e) plant leaf extract

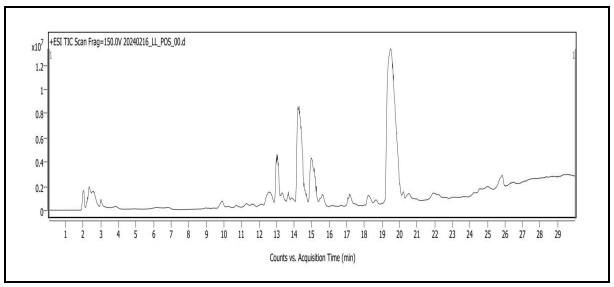


Fig. 16: LC-MS chromatogram of *K. fedtschenkoi* leaf extract showing identified peaks of bioactive compounds

Table 3. LC-MS-based metabolic profiling of *K. fedtschenkoi* leaf extract

S. No.	Compound Name	Molecular Mass (m/z)[a]	RT (min)[b]
1	1,3,7-Trimethyluric acid	210.0747	2.567
2	Picein	298.1040	10.692
3	Lampranthin II	727.1986	11.423
4	Dihydrozeatin riboside	353.1688	13.224
5	Delavirdine	456.1941	14.085
6	Aculeacin A	1078.5803	15.179
7	Hebevinoside IV	604.4349	15.707
8	p-Coumaroylputrescine	234.1367	17.535
9	Ampeloside Bs1	934.4768	18.654
10	(±)7-epi Jasmonic Acid	210.1259	18.686
11	Altretamine	210.1602	19.179
12	Atenolol	266.1624	24.454
13	Nadolol	309.1945	24.779
14	(2xi,6xi)-7-Methyl-3-methylene-1,2,6,7-octanetetrol	204.1363	25.836
15	Heteratisine	391.2346	27.150

[a]Molecular mass values were obtained using LC–ESI–QTOF–MS in positive mode.
[b]RT = Retention time in minutes.

4. DISCUSSION

Nanoparticles, defined by their minuscule size and expansive surface area-to-volume ratio, exhibit a plethora of unique physical, chemical, and biological properties (Patel *et al.* 2021). These properties make nanoparticles incredibly versatile and applicable across a wide array of fields, from biomedical sciences to environmental remediation (Sonawane *et al.* 2022; Shelke *et al.* 2023). In parallel, green synthesis methods have emerged as sustainable alternatives to conventional nanoparticle synthesis approaches (Gupta *et al.* 2023). Silver nanoparticles (AgNPs) have garnered substantial attention within the realm of nanotechnology due to their remarkable antimicrobial, anticancer, and catalytic capabilities (Hano *et al.* 2021; Nascimento *et al.* 2023; Arunachalam *et al.* 2014). Researchers delved into the antimicrobial properties of AgNPs synthesized using extracts from *Kalanchoe pinnata*, a species known for its medicinal properties (Aryan *et al.* 2021). Patra *et al.* (2017) and Khan *et al.* (2019) demonstrated promising antimicrobial activity of AgNPs against a spectrum of pathogens, confirming their use in fighting against diseases.

The characterization of Kf-L-AgNPs using various analytical techniques provided valuable insights into their structural and optical properties. After treating the silver nitrate solution with the plant extract, the intensity of brown color varied slightly across plant parts extract used for the reaction, suggesting differences in phytochemical content and reducing capacity among the different plant parts (Ijaz *et al*. 2022; Ghojavand *et al.* 2020), which may influence nanoparticle formation and yield. UV-Vis spectroscopy revealed a distinct SPR peak around 420 nm, which is characteristic of silver nanoparticles. This absorbance was consistently observed across all samples synthesized using different *Kalanchoe fedtschenkoi* plant part extracts (leaf, root, stem, flower, and fruit). All samples demonstrated increased absorbance between 420–450 nm, confirming the excitation of SPR. Conversely, a decline in absorbance beyond 500 nm was noted, indicating reduced SPR activity and minimal aggregation. In comparison to Kf-AgNPs and plant leaf extract, the silver nitrate solution and distilled water showed no absorption. These findings highlight the optical stability and colloidal nature of the biosynthesized nanoparticles, aligning well with other reported works (Elegbede *et al.* 2019); (Patil *et al.* 2017), (Kadam *et al.* 2024); (Sonawane *et al*. 2021). FESEM revealed morphological differences in silver nanoparticles synthesized using different *K. fedtschenkoi* plant part extracts, with spherical shapes predominating across all samples. These findings indicate that the type of plant part extract influences the nanoparticle size and morphology. The variation in size can be attributed to the differences in the phytochemical The particle size and distribution varied slightly depending on the plant part used, indicating that

the phytochemical composition of each extract influenced nanoparticle morphology. This result is consistent with the findings of Ghojavand *et al.* (2020) and Ijaz *et al.* (2022). DLS analysis displayed varying effective diameters among samples, reflecting size heterogeneity within the nanoparticle populations, a trend also noted in other studies (MacCuspie *et al.* 2011). The analysis of the Kf-L-AgNPs samples shows a mean zeta potential of -11.34 mV, indicating moderate stability, with sample-specific values ranging from -4.69 mV to -18.62 mV. The mean mobility of -0.89 µ/s/(V/cm) and the RMS residual values confirm consistent measurements with low variability, as reflected in the standard deviation of the RMS residual at 0.021838. Similar findings were emphasized by Shoaib *et al.* (2021) and Khane *et al.* (2022a). These findings highlight the stable dispersion and structural integrity of the biosynthesized nanoparticles, making them suitable for various applications. XRD analysis confirmed the formation of crystalline Kf-L-AgNPs, with distinct peaks at 2θ ≈ 38.1°, 44.3°, 64.4°, and 77.3°, corresponding to the (111), (200), (220), and (311) planes of face-centered cubic metallic silver (Ag^0). The absence of oxide-related peaks indicates that the phytochemicals in *K. fedtschenkoi* extract efficiently reduced Ag^+ ions to their elemental form without significant oxidation. The sharp and intense reflections indicate the high crystallinity of the nanoparticles, supporting earlier biosynthesis findings reported by Zaki *et al.* (2011) and Mukunthan *et al.* (2011). EDS confirmed elemental composition changes, with significant increases in silver content at higher concentrations. This result is in line with Ale *et al.* (2019). The unique absorption at 3 keV indicates the successful AgNP formation, which can be correlated with the studies conducted by Ingale *et al.* (2023). This comprehensive analysis further underscores the reliability and reproducibility of the green synthesis method, offering a promising route for tunable and stable silver nanoparticle production for potential biomedical and environmental applications. FTIR analysis of Kf-L-AgNPs revealed the presence of key functional groups involved in nanoparticle synthesis. The broad band at 3429.20 cm^{-1} corresponded to O–H stretching, indicating the role of phenolic compounds and flavonoids in reducing Ag^+ ions. Peaks at 2920.75 cm^{-1} and 2853.31 cm^{-1} were attributed to C–H stretching, suggesting the presence of organic stabilizers. The strong C=O stretching at 1700.81 cm^{-1} confirmed the involvement of proteins or carbonyl groups in capping. Additional peaks at 1241.20 cm^{-1}, 1129.86 cm^{-1}, and 1018.54 cm^{-1} indicated contributions from polysaccharides and C–O/C–N containing compounds, further supporting the role of plant biomolecules in nanoparticle stabilization. FTIR findings are showing consistency with the observations conducted by Sonawane *et al.* (2021), Sardar *et al.* (2007), and Kanipandian *et al.* (2014).

The IC_{50} values obtained for our Kf-L-AgNPs against MCF-7 cells (34.81 µg/mL) and A549 cells (98.73 µg/mL) are indicative of significant cytotoxicity, highlighting their promising anticancer properties. Comparing the results with the past research works, alignment and correlation were found, reinforcing the efficacy of Kf-L-AgNPs as potential anticancer agents (Abarca *et al.* 2016; Arunachalam *et al.* 2014 and Kanipandian *et al.* 2014). Several studies have investigated the cytotoxic effects of silver nanoparticles against various cancer cell lines, including breast and lung cancers, providing valuable insights into their therapeutic potential (Bandyopadhyay *et al.* 2020; Rakowski *et al.* 2021). One notable study (Kuraganti *et al.* 2020) explored the anticancer activity of AgNPs produced using the extract of *Chroococcus turgidus* against MCF-7 cells, reporting IC_{50} values in a similar range to the findings of the present study. Their research demonstrated dose-dependent cytotoxicity, with higher concentrations of Kf-L-AgNPs leading to increased inhibition of cell growth. This matches the observations of the present work and supports the notion that Kf-L-AgNPs exhibit significant anticancer effects against breast cancer cells.

Similarly, investigations into the cytotoxicity of AgNPs against lung cancer cells, such as the A549 cell line, have been documented in the literature. The reported IC_{50} values for AgNPs against A549 cells by Yontar *et al.* (2023) align closely with the obtained results. They observed dose-dependent cytotoxicity, with higher concentrations of AgNPs displaying pronounced inhibitory effects on cell viability. This concordance strengthens the evidence for AgNPs as potent anticancer agents, particularly against lung cancer cells. The comparison of Kf-L-AgNPs with docetaxel, a standard chemotherapeutic drug, revealed notable efficacy in reducing cell viability, particularly against MCF-7 cells. These results align with the findings of Al Saqr *et al.* (2021) and Ingale *et al.* (2023), who evaluated the cytotoxicity of AgNPs against breast cancer cells and found comparable IC_{50} values. The cytotoxicity results of Kf-L-AgNPs revealed their dose-dependent anticancer activity against MCF-7 and A549 cancer cell lines. However, it is acknowledged that the IC_{50} values for Kf-L-AgNPs (34.81 µg/mL for MCF-7 and 98.73 µg/mL for A549) are higher than those of the standard drug docetaxel (13.73 µg/mL for MCF-7 and 33.09 µg/mL for A549), suggesting that a higher concentration of Kf-L-AgNPs is required to achieve comparable anticancer effects. This higher concentration, while less potent than synthetic drugs, aligns with findings from other biogenic nanoparticles reported in the literature, where IC_{50} values often range from 25 µg/mL to 100 µg/mL depending on the cell line (Ratan *et al.* 2020).

The elevated IC_{50} values of Kf-L-AgNPs could be attributed to their biogenic origin and the stabilizing biomolecules from *K. fedtschenkoi* leaf extract, which may modulate their cytotoxicity. Despite this, the biocompatibility, reduced side effects, and natural origin

of Kf-L-AgNPs offer a distinct advantage over synthetic chemotherapeutic agents.

The results of the antimicrobial activity testing of Kf-L-AgNPs against *E. coli* and *S. aureus* reveal significant potential as antimicrobial agents. Our findings align with existing literature and highlight the efficacy of Kf-L-AgNPs in inhibiting the growth of these bacterial strains. Several studies have reported similar results regarding the antimicrobial activity of AgNPs. For example, a study by Vu *et al.* (2018) demonstrated the zone of inhibition for *E. coli* and *S. aureus* using AgNPs at a concentration of 1 mg/mL, which aligned with the current study's results. Furthermore, a concentration-dependent effect on antimicrobial activity was observed, which is consistent with the studies by Patra *et al.* (2017) and Kadam *et al.* (2024), demonstrating a similar trend in antimicrobial efficacy with increasing AgNPs concentrations.

The LC-MS analysis of *K. fedtschenkoi* leaves revealed a rich array of secondary metabolites, comparable to findings in other medicinal plants. (Ahmed *et al.* 2012; Stefanowicz-Hajduk *et al.* 2022).

Besides genus *Kalanchoe*, in other plant species, phenolic compounds such as picein and *p*-coumaroylputrescine, identified in the present study, have also been reported in the leaves of *Vitis vinifera* and *Picea glauca*, respectively (Allegro *et al*. 2021; Kraus *et al.* 1997). These phenolics are known for their antioxidant properties, which can enhance the stability and efficacy of synthesized nanoparticles, similar to the findings in *Azadirachta indica*, where phenolic content played a crucial role in nanoparticle stabilization (Ghosh *et al.* 2020). Flavonoids such as lampranthin II, detected in the analysis, are also found in *Amaranthus tricolor* and exhibit significant anti-inflammatory and anticancer activities (Hussain *et al.* 2018). In the context of nanoparticle synthesis, flavonoids are crucial as they act as both reducing and capping agents, enhancing the biomedical applications of nanoparticles, as observed in *Citrus limon-mediated* synthesis (Khane *et al*. 2022). The presence of jasmonic acid, a terpene, is notable as it has been observed in *Arabidopsis thaliana* and is known for its role in plant defense mechanisms and anti-inflammatory properties (Wang *et al.* 2021). Terpenes are vital in nanoparticle synthesis due to their ability to act as reducing agents, similar to their role in the green synthesis of gold nanoparticles using *Eucalyptus globulus* (Balčiūnaitienė *et al*. 2022).

Also, nitrogen-containing compounds like 1,3,7-trimethyluric acid and delavirdine have been previously identified in *Camellia sinensis* and *Hordeum vulgare*, respectively, and are recognized for their diverse bioactivities, including antimicrobial and antiviral effects (Jiang *et al.* 2021; Abajo *et al.* 2023). These nitrogen-containing compounds contribute significantly to the bioreduction processes in nanoparticle synthesis, enhancing their antimicrobial properties, as demonstrated in *Moringa oleifera*-mediated synthesis (Chaudhary *et al.* 2023). Complex molecules, including dihydrozeatin riboside and aculeacin A, highlight the extensive phytochemical profile of *K. fedtschenkoi*. Dihydrozeatin riboside, found in *Zea mays*, plays a critical role in cell division and growth, while aculeacin A, isolated from *Aspergillus* species, exhibits potent antifungal properties (Jameson *et al.* 2023) (Yodsing *et al.* 2018). These complex molecules are essential in nanoparticle synthesis, providing multifunctional properties to the nanoparticles, enhancing their applicability in various biomedical fields. These secondary metabolites have significance in plant defense mechanisms against herbivorous animals and microorganisms (Lokare *et al.* 2024). The identification of these compounds underscores the biochemical significance and biomedical potential of *Kalanchoe fedtschenkoi*, supporting its use in traditional medicine and highlighting its potential for developing new therapeutic agents.

5. CONCLUSION

This study reports the successful synthesis of silver nanoparticles (Kf-L-AgNPs) by the green method using *Kalanchoe fedtschenkoi* leaf extract, demonstrating an eco-friendly and sustainable alternative to conventional chemical synthesis methods. By various characterization techniques, it is clear that the Kf-L-AgNPs are spherical in shape with an average size of around 25 nm. The biological evaluation revealed that Kf-L-AgNPs possess effective cytotoxicity against MCF-7 breast cancer and A549 lung cancer cells, showing strong anticancer potential. The significant antimicrobial activity produces substantial zones of inhibition against *E. coli* and *S. aureus*, thereby demonstrating their potential to combat multidrug-resistant bacteria. The LC-MS profiling of *K. fedtschenkoi* leaf extract identified a diverse range of secondary metabolites, including phenolics, flavonoids, terpenes, saponins, and nitrogen-containing compounds, which play a dual role in both the biosynthesis and bio-functionalization of AgNPs. These bioactive molecules enhanced the biological performance of Kf-L-AgNPs. The synthesized Kf-L-AgNPs demonstrated excellent antibacterial and anticancer properties, along with strong physicochemical stability, making them promising candidates for future biomedical applications. The study reinforces the utility of medicinal plants like *K. fedtschenkoi* in nanotechnology and paves the way for the development of novel, plant-based nano-medicines targeting infectious diseases and cancer.

ACKNOWLEDGEMENTS

The authors are grateful to Loknete Ramdas Patil Dhumal Arts, Science & Commerce College,

Rahuri, Maharashtra, India, for providing the plants. The authors are highly thankful to Prof. Ramkrishna More College, Akurdi, Pune, India, and S. M. Joshi College, Hadapsar, Pune, India, for providing the laboratory facilities. The authors would also like to thank the Venture Center, CSIR-NCL, Pune, India, for the provision of the laboratory facility for antibacterial study.

FUNDING

This research received no specific grant from any funding agency in the public, commercial, or not-for-profit sectors.

CONFLICTS OF INTEREST

The authors declare that there is no conflict of interest.

COPYRIGHT

This article is an open-access article distributed under the terms and conditions of the Creative Commons Attribution (CC-BY) license (http://creativecommons.org/licenses/by/4.0/).

REFERENCES

Abajo, Z., Jimenez, A., Echaburu, -D. S., Valcárcel, Y., Segura, Y., Orive, G. and Lertxundi, U., Analyzing the Potential Environmental Impact of NIOSH List of Hazardous Drugs (Group 2), *Sci. Total Environ*., 873, 162280 (2023). https://doi.org/10.1016/j.scitotenv.2023.162280

Abarca, -V. R., Malacara, P. F. C. and Petricevich, L. V., Characterization of Chemical Compounds with Antioxidant and Cytotoxic Activities in Bougainvillea x Buttiana Holttum and Standl, (Var. Rose) Extracts, *Antioxid.*, 5(4), 45 (2016). https://doi.org/10.3390/antiox5040045

Ahmed, Sinthyia, and Habib, M. R., Analgesic and Neuropharmacological Activities of the Ethanolic Extract of Leaves of *Kalanchoe pinnata* (Lam.) Pers. in Swiss Albino Mice, *East West Univ*., 1-40 (2012)

Akhtar, J. M., Alhadlaq, A. H., Kumar, S., Alrokayan, A. S. and Ahamed, M., Selective Cancer-Killing Ability of Metal-Based Nanoparticles: Implications for Cancer Therapy, *Arch. Toxicol.*, 89 (11), 1895-1907 (2015). https://doi.org/10.1007/S00204-015-1570-1

Akter, M., Sikder, T. M., Rahman, M. M., Ullah, A. M. K. A., Hossain, B. F. K., Banik, S., Hosokawa, T., Saito, T. and Kurasaki, M., A Systematic Review on Silver Nanoparticles-Induced Cytotoxicity: Physicochemical Properties and Perspectives, *J. Adv. Res.*, 9, 1-16 (2018). https://doi.org/10.1016/J.JARE.2017.10.008

Ale, A., Liberatori, G., Vannuccini, M. L., Bergami, E., Ancora, S., Mariotti, G., Bianchi, N., Galdoporpora, M. J., Desimone, F. M., Cazenave, J. and Corsi, I., Exposure to a Nanosilver-Enabled Consumer Product Results in Similar Accumulation and Toxicity of Silver Nanoparticles in the Marine Mussel Mytilus Galloprovincialis, *Aquat. Toxicol.*, 211, 46-56 (2019). https://doi.org /10.1016/J.AQUATOX.2019.03.018

Ali., J., Ahmad, B. and Bashir, S., Optimization and Effects of Different Reaction Conditions for the Bioinspired Synthesis of Silver Nanoparticles Using Hippophae Rhamnoides Linn. Leaves Aqueous Extract, *World Appl. Sci. J*., 22(6), 836-843 (2013). https://doi.org/10.5829/idosi.wasj.2013.22.06.7394

Allegro, G., Pastore, C., Valentini, G. and Filippetti, I., The Evolution of Phenolic Compounds in Vitis Vinifera L. Red Berries during Ripening: Analysis and Role on Wine Sensory—A Review, *Agron*., 11 (5), 999 (2021). https://doi.org/10.3390/AGRONOMY11050999

Alves, T. O., D'Almeida, S. T. C., Scherf, A. K. and Ferreira, L. S. M., Modern Approaches in the Identification and Quantification of Immunogenic Peptides in Cereals by LC-MS/MS, *Front. Plant Sci.*, 10, 492083 (2019). https://doi.org/10.3389/FPLS.2019.01470/BIBTEX

Anand, U., Dey, A., Chandel, S. K. A., Sanyal, R., Mishra, A., Pandey, K. D., Falco, D. V., Upadhyay, A., Kandimalla, R., Chaudhary, A., Dhanjal, K. J., Dewanjee, S., Vallamkondu, J. and Lastra, J. M. P. D. L., Cancer Chemotherapy and beyond: Current Status, Drug Candidates, Associated Risks and Progress in Targeted Therapeutics, *Genes & Dis.*, 10 (4), 1367-1401 (2023). https://doi.org/10.1016/J.GENDIS.2022.02.007

Arunachalam, K. D., Arun, L. B., Annamalai, S. K. and Arunachalam, A. M., Potential Anticancer Properties of Bioactive Compounds of Gymnema Sylvestre and Its Biofunctionalized Silver Nanoparticles. *Int. J. Nanomed.*, 10(1), 31-41 (2015). https://doi.org/10.2147/IJN.S71182

Aryan, Ruby, and Mehata, M. S., Green Synthesis of Silver Nanoparticles Using *Kalanchoe pinnata* Leaves (Life Plant) and Their Antibacterial and Photocatalytic Activities, *Chem. Phy. Lett*., 778, 138760 (2021). https://doi.org/10.1016/J.CPLETT.2021.138760

Andrade, D. A. E., Machinski, I., Ventura, T. C. A., Barr, A. S., Pereira, V. A., Beltrame, L. F., Strangman, K. W. and Williamson, T. R., A Review of the Popular Uses, Anatomical, Chemical, and Biological Aspects of *Kalanchoe* (Crassulaceae): A Genus of Plants Known as 'Miracle Leaf', *Mol.,* 28(14), 5574 (2023) https://doi.org/10.3390/molecules28145574

Balčiūnaitienė, A., Liaudanskas, M., Puzerytė, V., Viškelis, J., Janulis, V., Viškelis, P., Griškonis, E. and Jankauskaitė, V., Eucalyptus Globulus and Salvia Officinalis Extracts Mediated Green Synthesis of Silver Nanoparticles and Their Application as an Antioxidant and Antimicrobial Agent, *Plants*, 11(8), 1085 (2022). https://doi.org/10.3390/plants11081085

Bandyopadhyay, A., Roy, B., Shaw, P., Mondal, P., Mondal, K. M., Chowdhury, P., Bhattacharya, S. and Chattopadhyay, A., Cytotoxic Effect of Green Synthesized Silver Nanoparticles in MCF7 and MDA-MB-231 Human Breast Cancer Cells in Vitro, *Nucleus,* 63(2) 191–202 (2020). https://doi.org/10.1007/S13237-019-00305-Z/METRICS

Boshuizen, J. and Peeper, S. D., Rational Cancer Treatment Combinations: An Urgent Clinical Need, *Perspect.*, 78(6), 1002-1018 (2020). https://doi.org/10.1016/j.molcel.2020.05.031

Casanova, J. M., Nascimento, S. D. B. L., Casanova, M. L., Castricini, D. S., Souza, D. E.E.J., Yien, K. M. R., Costa, S.S. and Tavares, S. E., *Kalanchoe fedtschenkoi* R. Hamet & H. Perrier, a Non-Conventional Food Plant in Brazil: HPLC-DAD-ESI-MS/MS Profile and Leaf Histochemical Location of Flavonoids, *J. Appl. Bot. Food Qual*., 95, 154 (2022). https://doi.org/10.5073/JABFQ.2022.095.020

Chaudhary, J., Jandu, S., Tailor, G. and Chetna, Green Synthesis and Characterization of Iron Nanoparticles Using Moringa Oleifera (Leaves) and Their Phytochemical Screening with Biological Significance, *Chem. Data Collect*., 47, 101065 (2023). https://doi.org/10.1016/j.cdc.2023.101065

Coutinho, M. A. S., Muzitano, F. M., Camargo, M. M. L. and Costa, S. S., Therapeutic Potential of *Kalanchoe* Species: Flavonoids and Other Secondary Metabolites, *Nat. Prod. Commun.*, 3(12) 2151–2164 (2008). https://doi.org/10.1177/1934578X0800301236

Das, B., Dash, S. K., Mandal, D., Ghosh, T., Chattopadhyay, S., Tripathy, S., Das, S., Dey, S. K., Das, D. and Roy, S., Green Synthesized Silver Nanoparticles Destroy Multidrug Resistant Bacteria via Reactive Oxygen Species Mediated Membrane Damage, *Arabian J. Chem.*, 10(6), 862-876 (2017). https://doi.org/10.1016/j.arabjc.2015.08.008

Lokare, D. P., Kumar, A., Bhaskar, K., Patra, K. K., Agrawal, S., Jadhav, S., Patil, N. D. and Khodade, H. H., A Cognitive Behavioral Defense Mechanism of Plants Against Herbivory, *Accessed,* 29(1), 49-55 (2023) https://doi.org/10.33451/florafauna.v29i1pp49-55

Elegbede, J. A. and Lateef, A., Green Synthesis of Silver (Ag), Gold (Au), and Silver–Gold (Ag–Au) Alloy Nanoparticles: A Review on Recent Advances, Trends, and Biomedical Applications, *Nanotechnol. Nanomater. Appl. Food, Health, Biomed. Sci.*, 1st Ed., 3–88 (2019). https://doi.org/10.1201/9780429425660-1

Almeida, C. F., Oliveira, A., Ramos, J. M., Fernandes, A. P., Teixeira, N. and Amaral, C., Estrogen Receptor-Positive (ER+) Breast Cancer Treatment: Are Multi-Target Compounds the next Promising Approach?, *Biochem. Pharmacol.,* 177, 113989 (2020). https://doi.org/10.1016/j.bcp.2020.113989

Gegengeimer, P., Preparation of Extracts from Plants. *Methods Enzymol*., 182, 174–93 (1990). https://doi.org/10.1016/0076-6879(90)82016-U

Ghojavand, S., Madani, M. and Karimi, J., Green Synthesis, Characterization and Antifungal Activity of Silver Nanoparticles Using Stems and Flowers of Felty Germander, *J. Inorg. Organomet. Polym. Mater.*, 30(8), 2987–97 (2020). https://doi.org/10.1007/S10904-020-01449-1/METRICS

Ghosh, T., Chattopadhyay, A., Mandal, C. A., Pramanik, S. and Kuiri, K. P., Optical, Structural, and Antibacterial Properties of Biosynthesized Ag Nanoparticles at Room Temperature Using Azadirachta Indica Leaf Extract, *Chin. J. Phys.*, 68, 835-848 (2020). https://doi.org/10.1016/j.cjph.2020.10.025

Gul, R., Naqib, S., Saleh, M. A. E., Khan, S. U., Ibrahim, M., Tabassum, S., Zaman, U., Rehman, U. K., Khan, D., Rizg, Y. W., Hosny, M. K., Alissa, M., Bukhary, M. S. and Alkhalidi, M. H., An Eco-Benign Biomimetic Approach for the Synthesis of Novel Silver Nanoparticles (Kt-AgNPs): Ultra Efficient Nanoparticles with Enhanced Biomedical Applications, *Inorg. Chem. Commun*., 155, 111109 (2023). https://doi.org/10.1016/j.inoche.2023.111109

Gupta, D., Boora, A., Thakur, A. and Gupta. K. T., Green and Sustainable Synthesis of Nanomaterials: Recent Advancements and Limitations, *Environ. Res.*, 231 (Part3), 116316 (2023). https://doi.org/10.1016/j.envres.2023.116316

Hano, C. and Abbasi, H. B., Plant-Based Green Synthesis of Nanoparticles: Production, Characterization and Applications, *Biomol.*, 12(1), 31 (2021). https://doi.org/10.3390/biom12010031

Hussain, E. A., Sadiq, Z. and Haq, -U. -Z. M., Betalains: Biomolecular Aspects, *Betalains: Biomol. Aspects*, 1st Ed., 1–187 (2018). https://doi.org/10.1007/978-3-319-95624-4

Ijaz, I., Bukhari, A., Gilani, E., Nazir, A., Zain, H., Saeed, R., Hussain, S., Hussain, T., Bukhari, A., Naseer, Y. and Aftab, R., Green Synthesis of Silver Nanoparticles Using Different Plants Parts and Biological Organisms, Characterization and Antibacterial Activity, *Environ. Nanotechnol*., 18, 100704 (2022). https://doi.org/10.1016/j.enmm.2022.100704

Ingale, S., Gaykar, B., Pagar, K. and Shelke, D., Green Synthesis of Silver Nanoparticles from Cyathocline Purpurea (Don) O. Kuntze and Its Efficacy Against MCF-7 Cancer Cell Line, *BioNanoSci*., 13(3), 1-16 (2023). https://doi.org/10.1007/s12668-023-01138-6

Jameson, E. P., Zeatin: The 60th Anniversary of Its Identification, *Plant Physiol.*, 192(1), 34–55 (2023). https://doi.org/10.1093/plphys/kiad094

Jamkhande, P. G., Ghule, N. W., Bamer, A. H. and Kalaskar. G. M., Metal Nanoparticles Synthesis: An Overview on Methods of Preparation, Advantages and Disadvantages, and Applications, *J. Drug Delivery Sci. Technol*., 53, 101174 (2019). https://doi.org/10.1016/j.jddst.2019.101174

Janikddfghx, E., Ceremuga, M., Niemcewicz, M. and Bijak, M., Dangerous Pathogens as a Potential Problem for Public Health, *Med.,* 56(11), 591 (2020). https://doi.org/10.3390/medicina56110591

Jiang, C. K., Liu, Z. L., Li, X. Y., Ercisli, S., Qiang, M. J. and Chen, L., Non-Volatile Metabolic Profiling and Regulatory Network Analysis in Fresh Shoots of Tea Plant and Its Wild Relatives, *Front. Plant Sci.*, 12 , 746972 (2021). https://doi.org/10.3389/fpls.2021.746972

Kadam, N. S., Shelke, B. D., Naik, A. A., Tak, R. D., Doshi, P. J. and Nikam, T. D., Sunlight and Microwave Catalyzed Comparative Biosynthesis of Silver Nanoparticles Using In-Vitro and in-Vivo Biomass of Fagonia Schweinfurthii Hadidi, Its Antibacterial Activity and Phytotoxicity, *Plant Nano Biol.,* 8, 100071 (2024). https://doi.org/10.1016/j.plana.2024.100071

Kanipandian, N., Kannan, S., Ramesh, R., Subramanian, P. and Thirumurugan, R., Characterization, Antioxidant and Cytotoxicity Evaluation of Green Synthesized Silver Nanoparticles Using Cleistanthus Collinus Extract as Surface Modifier, *Mater. Res. Bull.*, 49(1), 494–502 (2014). https://doi.org/10.1016/j.materresbull.2013.09.016

Khan, I., Saeed, K. and Khan, I., Nanoparticles: Properties, Applications and Toxicities, *Arabian J. Chem.,* 12(7), 908–31 (2019). https://doi.org/10.1016/j.arabjc.2017.05.011

Khan, M., Silver Nanoparticles - Fabrication, Characterization and Applications, *InTech*, 1-288 (2018). https://doi.org/10.5772/intechopen.71247

Khane, Y., Benouis, K., Albukhaty, S., Sulaiman, G. M., Abomughaid, M. M., Ali, A.A., Aouf, D., Fenniche, F., Khane, S., Chaibi, W., Henni, A., Bouras, H. D. and Dizge, N., Green Synthesis of Silver Nanoparticles Using Aqueous Citrus Limon Zest Extract: Characterization and Evaluation of Their Antioxidant and Antimicrobial Properties, *Nanomater.,* 12(12), 2013 (2022). https://doi.org/10.3390/nano12122013

Kraus, C. and Spiteller, G., Comparison of Phenolic Compounds from Galls and Shoots of Picea Glauca, *Phytochem.,* 44(1), 59–67 (1997). https://doi.org/10.1016/S0031-9422(96)00388-3

Kuraganti, G. S., Edla, S., Dasari, T. and Reddy, M., Characterization, in Vitro Cytotoxic and Antibacterial Exploitation of Green Synthesized Freshwater Cyanobacterial Silver Nanoparticles, *J. Appl. Pharm. Sci.,* 10(9), 088–098 (2020). https://doi.org/10.7324/JAPS.2020.10911

MacCuspie, R. I., Rogers, K., Patra, M., Suo, Z., Allen, J. A., Martin, N. M. and Hackley, A. V., Challenges for Physical Characterization of Silver Nanoparticles under Pristine and Environmentally Relevant Conditions, *J. Environ. Monit.*, 13(5), 1212–26 (2011). https://doi.org/10.1039/C1EM10024F

Mejía, M. J. L.., Bach, H., Leal, L. C. A., López, N. E. D., Mena, L. R. E., Hernández, R. L. and Arreola, S. E., Biological Activities and Chemical Profiles of *Kalanchoe fedtschenkoi* Extracts, *Plants*, 12(10), 1943 (2023). https://doi.org/10.3390/plants12101943

Molina, G. A., Esparza, R., Miranda, L. L. J., Martínez, -H. R. A., Sánchez, -E. L. B., Peña, -E. A. E. and Esteve, M., Green Synthesis of Ag Nanoflowers Using *Kalanchoe daigremontiana* Extract for Enhanced Photocatalytic and Antibacterial Activities, *Colloids Surf., B,* 180, 141–49 (2019). https://doi.org/10.1016/j.colsurfb.2019.04.044

Mourdikoudis, S., Pallares, R. M. and Thanh, T. K. N., Characterization Techniques for Nanoparticles: Comparison and Complementarity upon Studying Nanoparticle Properties, *Nanoscale,* 10(27), 12871–934 (2018). https://doi.org/doi:10.1039/C8NR02278J

Mukunthan, K. S., Elumalai, E. K., Patel, T. N. and Murty, R. V., Catharanthus Roseus: A Natural Source for the Synthesis of Silver Nanoparticles, *Asian Pac. J. Trop. Biomed.,* 1(4), 270–74 (2011). https://doi.org/10.1016/S2221-1691(11)60041-5

Murthy, H. C. A., Wagassa, A. N., Ravikumar, C. R. and Nagaswarup, H. P., Functionalized Metal and Metal Oxide Nanomaterial-Based Electrochemical Sensors, Principles, Fabrication Methods, and Applications, Woodhead Publishing Series in Electronic and Optical Materials*, Woodhead Publishing*, 369–92 (2022). https://doi.org/10.1016/B978-0-12-823788-5.00001-6

Nascimento, L. B. D. S., Casanova, L. M. and Costa, S. S., Bioactive Compounds from *Kalanchoe* Genus Potentially Useful for the Development of New Drugs, *Life,* 13(3), 646 (2023). https://doi.org/10.3390/life13030646

Netala, V. R., Hou, T., Sana, S. S., Li, H. and Zhang, Z., Rosmarinic Acid-Rich Perilla Frutescens Extract-Derived Silver Nanoparticles: A Green Synthesis Approach for Multifunctional Biomedical Applications Including Antibacterial, Antioxidant, and Anticancer Activities, *Mol.,* 2024, 29(6), 1250 (2024). https://doi.org/10.3390/molecules29061250

Patel, J. K.., Patel, A. and Bhatia, D., Introduction to Nanomaterials and Nanotechnology, *Emerging Technologies for Nanoparticle Manufacturing, Springer, Cham,* 3–23 (2021). https://doi.org/10.1007/978-3-030-50703-9_1

Patil, M. P., Palma, J., Simeon, N. C., Jin, X., Liu, X., Ngabire, D., Kim, N. H., Tarte, N. H. and Kim, G. D., Sasa Borealis Leaf Extract-Mediated Green Synthesis of Silver–Silver Chloride Nanoparticles and Their Antibacterial and Anticancer Activities, *New J. Chem.,* 41(3), 1363–71 (2017). https://doi.org/10.1039/C6NJ03454C

Patra, J. K. and Baek. K. H., Antibacterial Activity and Synergistic Antibacterial Potential of Biosynthesized Silver Nanoparticles against Foodborne Pathogenic Bacteria along with Its Anticandidal and Antioxidant Effects, *Front. Microbiol.*, 8, 227226 (2017). https://doi.org/10.3389/fmicb.2017.00167

Qu, G. P., Shi, M., Wang, D., Wu, J. H., Wang, P., Gong, M. L. and Zhang, Z. J., Dual Targeting of MEK and PI3K Effectively Controls the Proliferation of Human EGFR-TKI Resistant Non-Small Cell Lung Carcinoma Cell Lines with Different Genetic Backgrounds, *BMC Pulm. Med.,* 21(1), 1–12 (2021). https://doi.org/10.1186/S12890-021-01571-X/FIGURES/6

Rakowski, M., Porębski, S. and Grzelak, A., Silver Nanoparticles Modulate the Epithelial-to-Mesenchymal Transition in Estrogen-Dependent Breast Cancer Cells In Vitro, *Int. J. Mol. Sci.*, 22(17), 9203 (2021). https://doi.org/10.3390/ijms22179203

Ratan, Z. A., Haidere, M. F., Nurunnabi, M., Shahriar, S. M., Ahammad, A. J. S., Shim, Y. Y., Reaney, M. J. T. and Cho, J. Y., Green Chemistry Synthesis of Silver Nanoparticles and Their Potential Anticancer Effects, *Cancers,* 12(4), 855 (2020). https://doi.org/10.3390/cancers12040855

Raut, R. W., Kolekar, N. S., Lakkakula, J. R., Mendhulkar, V. D. and Kashid, S. B., Extracellular Synthesis of Silver Nanoparticles Using Dried Leaves of Pongamia Pinnata (L) Pierre, *Nano-Micro Lett.,* 2(2), 106–13 (2010). https://doi.org/10.1007/BF03353627

Rónavári, A., Igaz, N., Adamecz, D. I., Szerencsés, B., Molnar, C., Kónya, Z., Pfeiffer, I. and Kiricsi, M., Green Silver and Gold Nanoparticles: Biological Synthesis Approaches and Potentials for Biomedical Applications, *Mol.,* 26(4), 1–39 (2021). https://doi.org/10.3390/molecules26040844

Saqr, A. A., Wani, S. U. D., Gangadharappa, H. V., Aldawsari, M. F., Khafagy, S. E., Lila, A. S. A., Enhanced Cytotoxic Activity of Docetaxel-Loaded Silk Fibroin Nanoparticles against Breast Cancer Cells, *Polym.,* 13(9), 1416 (2021). https://doi.org/10.3390/polym13091416

Sardar, R., Park, J. W. and Parry, -S. S. J., Polymer-Induced Synthesis of Stable Gold and Silver Nanoparticles and Subsequent Ligand Exchange in Water, Langmuir, 23(23), 11883–89 (2007). https://doi.org/10.1021/LA702359G/SUPPL_FILE/LA702359G-FILE002.PDF

Sofi, A. M., Sunitha, S., Ashaq, S. M., Pasha, K. K. S. and Choi, D., An Overview of Antimicrobial and Anticancer Potential of Silver Nanoparticles, *J. King Saud Univ. - Sci*., 34(2), 101791 (2022). https://doi.org/10.1016/j.jksus.2021.101791

Sengul, A. B. and Asmatulu, E., Toxicity of Metal and Metal Oxide Nanoparticles: A Review, *Environ. Chem. Lett.,* 18(5), 1659–83 (2020). https://doi.org/10.1007/S10311-020-01033-6

Shah, W. H., Saleem, S., Mushtaq, N. U., Rasool, A., Tahir, I. and Rehman, R. U., C4 and CAM Plants with Better Resilience to Environmental Stresses, Photosynthesis and Respiratory Cycles during Environmental Stress Response in Plants, 1st Ed., *Apple Academic Press*, 163–91 (2022). https://doi.org/10.1201/9781003315162-8

Shelke, D. B., Islam, N. F., Chambhare, M. R., Sonawane, H. B., Patowary, R., Prasad, R. and Sarma, H., Enhancing Secondary Metabolites and Alleviating Environmental Stress in Crops with Mycogenic Nanoparticles: A Comprehensive Review, *Biocatal. Agric. Biotechnol.,* 52(x), 102805 (2023). https://doi.org/10.1016/j.bcab.2023.102805

Shoaib, M., Naz, A., Osra, F. A., Abro, S. H., Qazi, S. U., Siddiqui, F. A., Shah, M. R. and Mirza, A. Z., Green Synthesis and Characterization of Silver-Entecavir Nanoparticles with Stability Determination, *Arabian J. Chem.,* 14(3), 102974 (2021). https://doi.org/10.1016/j.arabjc.2020.102974

Singh, S., Arkoti, N. K., Verma, V. and Pal, K., Nanomaterials and Their Distinguishing Features, *Nanomater. Adv. Technol*., xx(x), 1–18 (2022). https://doi.org/10.1007/978-981-19-1384-6_1

Smith, G. F., A Review of the Ecology and Natural History of *Kalanchoe* (Crassulaceae Subfam. Kalanchooideae) in Southern Africa, 2022(40), 161–84 (2022). https://doi.org/10.25223/brad.n40.2022.a15

Smith, G. F. and Shtein, R., A Review of Horticulturally Desirable Characters in *Kalanchoe* (Crassulaceae Subfam. Kalanchooideae): Variable and Deviating Vegetative and Reproductive Morphologies Useful in Breeding Programmes, *Haseltonia,* 28(1), 106–19 (2022). https://doi.org/10.2985/026.028.0110

Sonawane, H., Arya, S., Math, S. and Shelke, D., Myco-Synthesized Silver and Titanium Oxide Nanoparticles as Seed Priming Agents to Promote Seed Germination and Seedling Growth of Solanum Lycopersicum: A Comparative Study, *Int. Nano Lett.,* 11(4), 371–79 (2021). https://doi.org/10.1007/s40089-021-00346-w

Sonawane, H., Shelke, D., Chambhare, M., Dixit, N., Math, S., Sen, S., Borah, S. N., Islam, N. F., Joshi, J. S., Yousaf, B., Rinklebe, J. and Sarma, H., Fungi-Derived Agriculturally Important Nanoparticles and Their Application in Crop Stress Management – Prospects and Environmental Risks, *Environ. Res*., 212, 113543 (2022) https://doi.org/10.1016/j.envres.2022.113543

Song, G., Guo, G., Du, T., Li, X., Wang, J., Yan, Y. and Zhao, Y., RALY May Cause an Aggressive Biological Behavior and a Dismal Prognosis in Non-Small-Cell Lung Cancer, *Exp. Cell Res.,* 389(2), 111884 (2020). https://doi.org/10.1016/J.YEXCR.2020.111884

Stefanowicz, -H. J., Hering, A., Gucwa, M., Achranowicz, S. K., Kowalczyk, M., Soluch, A. and Ochocka, R. J., An In Vitro Anticancer, Antioxidant, and Phytochemical Study on Water Extract of *Kalanchoe daigremontiana* Raym.-Hamet and H. Perrier, *Mol.,* 27(7), 2280 (2022). https://doi.org/10.3390/molecules27072280

Tee, J. K., Ong, C. N., Bay, B. H., Ho, H. K. and Leong, T. D., Oxidative Stress by Inorganic Nanoparticles, *Wiley Interdiscip. Rev.: Nanomed, Nanobiotechnol.*, 8(3), 414–38 (2015). https://doi.org/10.1002/wnan.1374

Uddin, T. M., Chakraborty, A. J., Khusro, A., Zidan, B. M. R. M., Mitra, S., Emran, T. B., Dhama, K., RIPON, H. K. M., Gajdacs, M., Sahibzada, K. U. M., Hossain, J. M. and Koirala, N., Antibiotic Resistance in Microbes: History, Mechanisms, Therapeutic Strategies and Future Prospects, *J. Infect. Public Health.,* 14(12), 1750–66 (2021). https://doi.org/10.1016/j.jiph.2021.10.020

Vu, X. H., Duong, T. T. T., Pham, T. T. H., Trinh, D. K., Nguyen, X. H. and Dang, V. S., Synthesis and Study of Silver Nanoparticles for Antibacterial Activity against *Escherichia coli* and *Staphylococcus aureus*, *Adv. Nat. Sci.: Nanosci. Nanotechnol.*, 9(2), 025019 (2018). https://doi.org/10.1088/2043-6254/AAC58F

Wang, Y., Mostafa, S., Zeng, W. and Jin, B., Function and Mechanism of Jasmonic Acid in Plant Responses to Abiotic and Biotic Stresses, *Int. J. Mol. Sci.,* 22(16), 8568 (2021). https://doi.org/10.3390/ijms22168568

Yaraki, M. T., Nasab, S. Z., Zare, I., Dahri, M., Sadeghi, M. M., Koohi, M. and Tan, Y. N., Biomimetic Metallic Nanostructures for Biomedical Applications, Catalysis, and Beyond, *Ind. Eng. Chem. Res.,* 61(22), 7547–93 (2022). https://doi.org/10.1021/acs.iecr.2c00285

Yin, R., Agrawal, T., Khan, U., Gupta, G. K., Rai, V., Huang, Y. Y. and Hamblin, M. R., Antimicrobial Photodynamic Inactivation in Nanomedicine: Small Light Strides Against Bad Bugs, *Nanomed*, 10(15), 2379–2404 (2015). https://doi.org/10.2217/nnm.15.67

Yodsing, N., Lekphrom, R., Sangsopha, W., Aimi, T. and Boonlue, S., Secondary Metabolites and Their Biological Activity from Aspergillus Aculeatus KKU-CT2, *Current Microbiol.,* 75(5), 513–18 (2018). https://doi.org/10.1007/s00284-017-1411-y

Yontar, A. K. and Çevik, S., Bio-Synthesized Silver Nanoparticles Using Cannabis Sativa Seed Extracts and Its Anticancer Effects, *Plasmonics,* 19(4), 1–13 (2023). https://doi.org/10.1007/S11468-023-02142-Y

Zaki, S., Kady, M. F. E. and Haleem, E. A. D., Biosynthesis and Structural Characterization of Silver Nanoparticles from Bacterial Isolates, *Mater. Res. Bull.,* 46(10), 1571–76 (2011). https://doi.org/10.1016/j.materresbull.2011.06.025